

WALLABY Pre-Pilot and Pilot Survey: the Tully Fisher Relation in Eridanus, Hydra, Norma and NGC4636 fields

Hélène M. Courtois^{1*}, Khaled Said^{2†}, Jeremy Mould^{3‡}, T.H. Jarrett⁴, Daniel Pomarède⁵, Tobias Westmeier^{6,7}, Lister Staveley-Smith^{6,7}, Alexandra Dupuy¹, Tao Hong⁸, Daniel Guinet¹, Cullan Howlett², Barbara Catinella^{6,7}, Nathan Deg⁹, Bi-Qing For⁶, Dane Kleiner¹⁰, Bärbel Koribalski^{11,12}, Karen Lee-Waddell^{6,15}, Kristine Spekkens¹³, Jing Wang¹⁴, O.I. Wong^{15,6,7}, Franck Bigiel¹⁶, Albert Bosma¹⁷, Matthew Colless¹⁸, Tamara Davis², Benne Holwerda¹⁹, Igor Karachentsev²⁰, Renée C. Kraan-Korteweg⁴, Kristen B.W. McQuinn²¹, Gerhardt Meurer⁶, Danail Obreschkow^{6,7}, Edward Taylor³

¹University Lyon 1, IUF, IP2I Lyon, 69622 Villeurbanne cedex, France

²School of Mathematics and Physics, The University of Queensland, Brisbane, QLD 4072, Australia

³Centre for Astrophysics & Supercomputing, Swinburne University, Australia

⁴Astronomy Department, University of Cape Town, Private Bag X3, Rondebosch, 7701, South Africa

⁵IRFU, CEA Université Paris-Saclay, 91191 Gif-sur-Yvette, France

⁶International Centre for Radio Astronomy Research (ICRAR), The University of Western Australia, M468, Crawley, WA 6009, Australia

⁷ARC Centre of Excellence for Astrophysics in 3 Dimensions (ASTRO 3D), Australia

⁸National Astronomical Observatories, Chinese Academy of Sciences, 20A Datun Road, Chaoyang District, Beijing 100012, China

⁹Department of Physics, Engineering Physics and Astronomy Queen's University Kingston, ON K7L 3N6, Canada

¹⁰INAF - Osservatorio Astronomico di Cagliari, Via della Scienza 5, 09047 Selargius, CA, Italy

¹¹Australia Telescope National Facility, CSIRO Astronomy and Space Science, P.O. Box 76, NSW 1710, Epping, Australia

¹²Western Sydney University, Locked Bag 1797, Penrith, NSW 2751, Australia

¹³Royal Military College of Canada, PO Box 17000, Station Forces, Kingston, Ontario, Canada K7K7B4

¹⁴Kavli Institute for Astronomy and Astrophysics, Peking University, Beijing 100871, China

¹⁵CSIRO Space & Astronomy, PO Box 1130, Bentley, WA 6102, Australia

¹⁶Argelander-Institut für Astronomie, Universität Bonn, Auf dem Hügel 71, 53121 Bonn, Germany

¹⁷Aix Marseille Univ, CNRS, CNES, LAM, Marseille, France

¹⁸Research School of Astronomy and Astrophysics, Australian National University, Canberra, ACT 2611, Australia

¹⁹University of Louisville, Department of Physics and Astronomy, 102 Natural Science Building, 40292 KY Louisville, USA

²⁰Special Astrophysical Observatory, Russian Academy of Sciences, Russia

²¹Rutgers University, Department of Physics and Astronomy, 136 Frelinghuysen Road, Piscataway, NJ 08854, USA

Accepted XXX. Received YYY; in original form ZZZ

ABSTRACT

The WALLABY pilot survey has been conducted using the Australian SKA Pathfinder (ASKAP) towards four fields in the Laniakea supercluster, partly near the Great Attractor. This region currently lacks sufficient numbers of accurate measurements of galaxy peculiar velocities, required for studies of bulk flow and gravitational field reconstruction. The pilot survey data are in the direction of the Eridanus, Hydra, Norma and NGC 4636 clusters, and consist of 614 galaxy spectra at a rest wavelength of 21cm. Of these spectra, 472 are of high enough quality to be used to potentially derive distances using the Tully-Fisher relation. We further restrict the sample to the 250 galaxies whose inclination is sufficiently close to edge-on (major to minor axis ratio $b/a < 0.7$). For these, we derive Tully-Fisher distances using the deprojected WALLABY velocity widths combined with infrared (WISE W1) magnitudes. This is the the first significant catalogue of galaxy distances from an SKA precursor interferometer, and allows a proof-of-concept comparison with previous single-dish studies. Tully-Fisher distances for the Eridanus, Hydra, Norma and NGC 4636 clusters are 21.5, 53.5, 69.4 and 23.0 Mpc respectively, with uncertainties of 5–10%.

The pilot survey data shows the benefits of WALLABY over previous giant single-dish telescope surveys due to the combination of sensitivity, field-of-view and freedom from terrestrial radio frequency interference. We estimate that WALLABY will permit a doubling of maximum survey distance and a tripling of the number of galaxies with Tully-Fisher distances.

Key words: surveys – radio astronomy: 21 cm – galaxies: distances and redshifts – cosmology: large-scale structure of Universe

* E-mail: helene.courtois@univ-lyon1.fr

† E-mail: k.saidahmedsoliman@uq.edu.au

1 INTRODUCTION

Brent Tully and Richard Fisher (Tully & Fisher 1977) discovered a relation (the Tully-Fisher relation: TFR) between the extensive properties of disk galaxies (mass, luminosity, and radius) and rotation velocity, which can be derived from the velocity width of their neutral hydrogen 21 cm spectra. If galaxy surface brightness, stellar mass, and mass to light ratio are functions of halo mass, the virial theorem leads one to expect a luminosity – rotation velocity relation. As the TFR relates distance-independent and distance-dependent quantities, it can be used to measure galaxy distances and peculiar velocities. Developments in understanding galaxy scaling relations are reviewed by Mould (2020). The TFR is also reproduced in dark matter simulations, when sub-grid physics is added to follow the baryons (e.g. Springel et al. 2018), so it can therefore also be used to further probe the astrophysics of galaxy formation.

The Widefield ASKAP L-band Legacy All-sky Blind Survey (WALLABY) pre-pilot and pilot phase 1 survey is an observational study of four fields with the Australian Square Kilometer Array Pathfinder (ASKAP) telescope. The pilot observations are a precursor to the full WALLABY survey, a blind neutral hydrogen survey of the Southern hemisphere (Koribalski et al. 2020) which is scheduled to begin in 2022. The pilot data has already been used to study HI content of galaxies in groups (For et al. 2021), discover dark clouds in the vicinity of galaxies (Wong et al. 2021), and study the diversity of ram pressure stripping of HI gas in galaxies in the Hydra cluster (Wang et al. 2021).

The raw ASKAP visibilities from the WALLABY observations are processed and reduced using ASKAPsoft. The processed data products are available on CASDA and released to the general public as WALLABY science data. A mosaic of individual footprints is then made to produce the final full sensitivity cubes which are run through the SoFiA pipeline. SoFiA is a 3D source finding and parametrisation software package (Serra et al. 2015; Westmeier et al. 2021) which, amongst many other outputs, produces a 1-dimensional spectrum by spatially integrating all emission within its mask. The measured HI linewidth is a measure of the galaxy projected rotation velocity.

In this article we explore the infrared TFR, by combining WALLABY pilot HI spectra with photometric data using WISE W1 band infrared fluxes. Infrared wavelengths have the advantage of markedly lower extinction of galaxy radiation by dust (Aaronson et al. 1979). It is now well known that using infrared data provides a tighter TFR than using optical bands (Sorce et al. 2013; Neill et al. 2014; Kourkchi et al. 2020b). The measured galaxy distances can be used to: measure the expansion rate through determination of the Hubble constant (Kourkchi et al. 2020b); test the Λ CDM cosmological model using measurements of the bulk flow (Hoffman et al. 2015; Hong et al. 2019); compute systematics in the SNIa Hubble constant determination (Peterson et al. 2021). Another question that measurements of non-Hubble flows can address is the quantity of matter needed in specific regions such as the Great Attractor in order to explain gravitationally-induced motions, with the aim of reconciling with observed baryonic matter distribution (Said et al. 2020; Thévenot et al. 2020).

A major benefit of the WALLABY survey is its higher sensitivity compared to previous southern surveys used for Tully-Fisher distances – for example, the HI Parkes All-Sky Survey (HIPASS) (Koribalski et al. 2004; Meyer et al. 2004). It also has higher survey speed than northern single-dish telescopes previously used to conduct HI surveys (Haynes et al. 2018) thanks to its wide (30 sq.deg)

Table 1. Table of J2000 coordinates pointings of the WALLABY pre-pilot and pilot phase 1 survey fields.

| Footprint | Field centre (J2000) | |
|------------|----------------------|--------------|
| | RA | DEC |
| Eridanus A | 03:39:30.000 | -22:23:00.00 |
| Eridanus B | 03:36:44.520 | -22:37:54.69 |
| Hydra-1A | 10:15:47.844 | -27:22:27.66 |
| Hydra-1B | 10:17:49.958 | -27:49:24.30 |
| Hydra-2A | 10:39:24.238 | -27:22:27.66 |
| Hydra-2B | 10:41:26.352 | -27:49:24.30 |
| NGC4636-1A | 12:38:02.328 | -00:26:59.95 |
| NGC4636-1B | 12:39:50.337 | -00:53:59.85 |
| NGC4636-2A | 12:38:02.729 | +04:56:58.64 |
| NGC4636-2B | 12:39:51.059 | +04:29:58.13 |
| Norma-1A | 16:16:30.928 | -59:27:41.88 |
| Norma-1B | 16:20:06.332 | -59:54:30.90 |
| Norma-2A | 16:55:26.063 | -59:27:41.88 |
| Norma-2B | 16:59:01.467 | -59:54:30.90 |

instantaneous field of view, thus enabling larger galaxy samples. Other advantages are the location of ASKAP at a site that is free from terrestrial radio frequency interference and its high angular resolution, which allows detailed morphological and dynamical studies. Although angular resolution is not important for this TFR study, it does lessen the probability of beam confusion and will allow future dynamical measurements of inclination.

All-sky infrared surveys provide complementary data for large samples of galaxies with a depth, resolution and photometric accuracy suitable for TFR studies. Examples include the 2MASS Tully-Fisher (2MTF) survey of 2,062 galaxies (Hong et al. 2019) and the WISE Tully-Fisher study of Lagattuta et al. (2013). Currently the largest Tully-Fisher samples are of the order of 10,000 galaxies (Kourkchi et al. 2020b), while WALLABY is planned to triple or more this latter number in the next few years (Koribalski et al. 2020).

Galaxy distances are key to the objective of the CosmicFlows (CF) project (Tully et al. 2016), which is to improve the cosmography of the nearby universe including the location and mass measurement of the largest attractors. Distances are used to compute velocity deviations from the Hubble cosmic expansion which are assumed to arise from the large-scale gravitational field. This can only be realized with very accurate distances. The CF project started in 2006 and will shortly publish its fourth generation catalogue containing about 45,000 accurate determinations of galaxy distances.

In this paper we describe the pre-pilot and phase 1 pilot WALLABY surveys from which our HI data is drawn, and present optical identifications of the detected sources at 21 cm (§2); we form TFRs by computing accurate photometry in the WISE W1 bandpass (§3). Finally, we show how the WALLABY Survey can add to the CF database for future studies of large-scale structure.

2 WALLABY PRE-PILOT AND PILOT SURVEY

WALLABY is an extragalactic all-sky HI survey with the ASKAP telescope which consists of 36×12 m dishes with baselines ranging from 22 m to 6 km (Hotan et al. 2021). It is equipped with phased array feeds with a field-of-view of about 30 deg^2 at 1.4 GHz. The frequency coverage of ASKAP is 0.7 to 1.8 GHz with an instantaneous bandwidth of 288 MHz. Its spectral resolution of 18.5 kHz translates into a velocity resolution of 4 km s^{-1} at redshift zero.

‡ E-mail: jmould@swin.edu.au

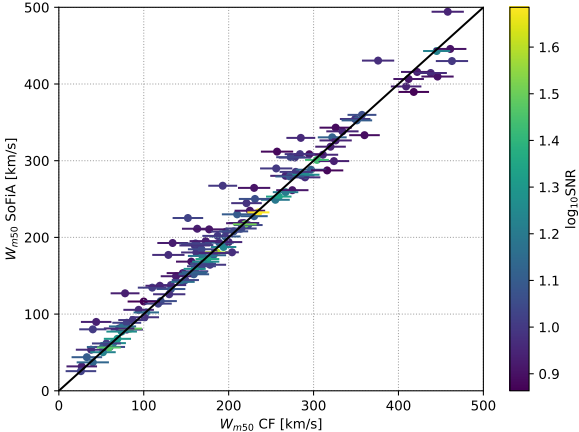


Figure 1. Linewidths $W_{\text{m}50}$ in the Norma field as measured by the CosmicFlows (CF) algorithm (labelled WALLABY on the plot) compared with the automatic measurements of SoFiA, colour-coded by S/N ratio. The plot only includes spectra with an error on $W_{\text{m}50}$ less or equal to 20 km s^{-1} . Two further spectra with low S/N ratio spectra, where the linewidth difference exceeds 100 km s^{-1} , are excluded from the plot.

For the WALLABY pilot surveys, a bandwidth of 144 MHz covering the frequency range of 1295.5 to 1439.5 MHz, was processed and imaged. This corresponds to redshifts $z < 0.096$. All baselines, including the 6 km baselines, were calibrated. However, the current WALLABY images only include baselines up to 2 km, resulting in an angular resolution of $30''$. The nominal RMS noise level is approximately 1.6 mJy after 2 footprints, each of duration 8 h, are combined. We refer the reader to [Koribalski et al. \(2020\)](#) for more details about the WALLABY survey.

2.1 Radio and photometry data measurements

The pre-pilot and pilot phase 1 survey resulted in coverage of the NGC4636 group, the Eridanus super-group, the Hydra I cluster, and the Norma cluster surrounds (the actual Norma cluster is excluded from this study due to strong residual radio continuum emission). Sources were catalogued using the SoFiA source finding pipeline ([Serra et al. 2015](#); [Westmeier et al. 2021](#)). Detections were linked across a spatial and spectral radius of 2 pixels with a minimum size requirement for reliable source identification of 5 spatial pixels and 8 spectral channels. SoFiA's reliability filter was then applied to remove all detections with a reliability below 0.8, using a Gaussian kernel density estimator of size 0.35 times the covariance. All remaining sources were then parameterised, assuming a restoring beam size of $30''$ for all integrated flux measurements. The source detection details slightly vary between the four different fields – details will be provided in the upcoming paper accompanying the first public data release of phase 1 pilot data.

The pre-pilot field containing the Eridanus super group was observed with two interleaving footprints (A and B) with an offset of $38'$, and rotated by a position angle of 45 deg relative to a standard ASKAP footprint. The Norma, Hydra and NGC4636 pilot observations were of two adjacent 30 sq.deg overlapping tiles (1 and 2) with the tile centres separated by 5.4 deg . Each tile consisted of two slightly offset footprints observed for 8 hours. Therefore, each 1-D HI spectrum has an effective integration time of 16 hr. The centres of the footprints are given in Table 1.

2.2 Comparison of velocity width measurement algorithms

SoFiA provides approximate linewidths for all galaxies that it finds in WALLABY cubes. However, to improve robustness, accuracy, reliability and compatibility with previous measurements, we also compute linewidths using the CF methodology and make a detailed comparison with the SoFiA estimates. The CF linewidth $W_{\text{m}50}$, is measured at the flux level that is 50% of the mean flux, averaged in channels within the wavelength range enclosing 90% of the total integrated flux ([Courtois et al. 2011a,b](#)). It is followed by a correction for redshift and instrumental broadening: $W_{\text{m}50}^{\text{corr}} = (W_{\text{m}50} - 2\Delta v\lambda)/(1+z)$, where z is the redshift in the CMB frame, Δv is the smoothed spectral resolution, and $\lambda = 0.25$ is an empirically determined constant ([Courtois et al. 2009](#)). The observed line width was also adjusted by separating out the broadening from turbulent motions and offsets to produce an approximation to $2V_{\text{max}}$, where $V_{\text{max}} = W_{\text{mx}}/2$ correspond to the rotation rate over the main body of a galaxy. [Tully & Fouqué \(1985\)](#) define the parameter W_{mx} as:

$$W_{\text{mx}}^2 = W_{\text{m}50}^{\text{corr},2} + W_{\text{t,m}50}^2 \left[1 - 2e^{-(W_{\text{m}50}^{\text{corr}}/W_{\text{c,m}50})^2} \right] - 2W_{\text{m}50}^{\text{corr}} W_{\text{t,m}50} \left[1 - e^{-(W_{\text{m}50}^{\text{corr}}/W_{\text{c,m}50})^2} \right]. \quad (1)$$

The parameters $W_{\text{c,m}50} = 100 \text{ km s}^{-1}$ and $W_{\text{t,m}50} = 9 \text{ km s}^{-1}$ are set following tests conducted in [Courtois et al. \(2009\)](#), and characterize respectively the transition from boxcar to Gaussian intrinsic profiles, and the turbulent broadening for the observed linewidth considered. It is then related to the rotation rate V_{max} by:

$$V_{\text{max}} = \frac{W_{\text{mx}}}{2 \sin(i)}, \quad (2)$$

where i is the inclination of the galaxy from face-on relative to the observer.

Details regarding the $W_{\text{m}50}$ and W_{mx} line width parameters and comparisons with alternatives are discussed in [Courtois et al. \(2009\)](#). A comparison of the CF and SoFiA linewidth measurements is shown in Figure 1.

We make a further comparison with velocity widths derived using the method described by ([Said et al. 2016](#), hereafter S16). This algorithm requires prior knowledge of the left and right horns which is currently done manually and returns the linewidth measured at 50% of the mean flux and its associated uncertainty estimated using MC error estimation. In addition, this algorithm returns linewidth measurements at 20% and 50% of the peak flux, 50% of the peak flux measured from a straight-line fit to both sides of the profile, and 50% of the peak flux measured at each of the two peaks, along with their associated MC errors. In this paper, we only compare the CF linewidth with the S16 linewidth measured at 50% of the mean flux, as shown in Fig. 2.

We use the relative error between pairs of measurements to quantitatively check for any large discrepancies between 50% widths measured with the CF algorithm and widths measured at 50% of the mean flux with the S16 algorithm. We used the pairwise relative error of the form:

$$\varepsilon = \frac{W_{\text{m}50}^{\text{CF}} - W_{\text{m}50}^{\text{S16}}}{\sqrt{(eW_{\text{m}50}^{\text{CF}})^2 + (eW_{\text{m}50}^{\text{S16}})^2}}, \quad (3)$$

where $W_{\text{m}50}^{\text{CF}}$, $W_{\text{m}50}^{\text{S16}}$, $eW_{\text{m}50}^{\text{CF}}$, and $eW_{\text{m}50}^{\text{S16}}$ are the 50% widths measurements from CosmicFlows and S16 algorithms and their associated statistical uncertainties, respectively. Values of ε for all galaxies are

Table 2. All galaxies with pairwise relative error $|\epsilon| > 1.0$ between the CosmicFlows and S16 algorithms.

| name | PGC | W_{m50} | e_{Wm50} | W_{m50}^{S16} | e_{Wm50}^{S16} | ϵ |
|----------------|-------|-----------|------------|-----------------|------------------|------------|
| J102439-244547 | 30532 | 94 | 18 | 112 | 2 | -1.0177 |
| J102447-264054 | 30545 | 271 | 17 | 322 | 13 | -2.4078 |
| J103442-283406 | 31296 | 247 | 15 | 263 | 4 | -1.0149 |
| J103726-261843 | 31557 | 199 | 18 | 224 | 2 | -1.3854 |
| J104127-275119 | 31842 | 99 | 19 | 119 | 5 | -1.0091 |
| J104142-284653 | 31855 | 107 | 15 | 128 | 7 | -1.2566 |
| J104513-262755 | | 50 | 17 | 74 | 6 | -1.3571 |
| J104905-292232 | 32361 | 117 | 17 | 142 | 3 | -1.4259 |
| J163452-603705 | 58536 | 189 | 17 | 215 | 1 | -1.5087 |
| J164359-600237 | | 215 | 18 | 244 | 17 | -1.1702 |
| J165105-585918 | 59112 | 84 | 14 | 114 | 3 | -2.0721 |
| J165145-590915 | | 71 | 18 | 90 | 5 | -1.0111 |

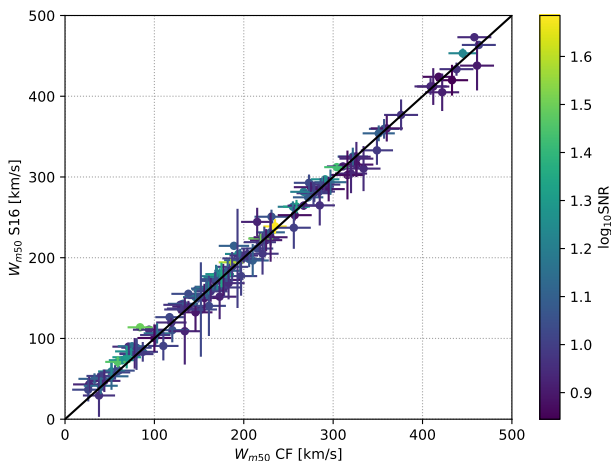


Figure 2. Comparison of 50% linewidths in the Norma field measured with the CF algorithm and linewidths measured at 50% of the mean flux using the S16 algorithm (Said et al. 2016). Only measurements of spectra with an adequate quality are displayed (error on W_{m50} less or equal to 20 km s^{-1}). This comparison confirms the internal robustness of the W_{m50} measurements, with a typical scatter at 20 km s^{-1} .

within the distribution of a Gaussian with a mean of zero and a standard deviation of unity. Table 2 lists all discrepant measurements with $|\epsilon| > 1.0$.

Following the CosmicFlows collaboration, the signal to noise flux ratio is computed as the ratio of the HI signal at 50% of the mean flux over the noise mean flux measured beyond the extremities of the HI line (Courtois & Tully 2015). It is not trivial to transfer this definition onto the 3D WALLABY spectra projected onto 1 dimension spectra since the mask size changes with frequency (and forces the noise to be zero beyond the mask). To be able to work with 1D SoFiA spectra we set the signal to noise value equal to the maximum flux level in the HI line.

The error on the linewidth e_W , follows the empirical relation from (Courtois et al. 2009):

$$\begin{aligned} \text{SNR} \geq 17 \quad e_W &= 8; \\ 2 < \text{SNR} < 17 \quad e_W &= 21.6 - 0.8 \text{ SNR}; \\ \text{SNR} \leq 2 \quad e_W &= 70 - 25 \text{ SNR}, \end{aligned} \quad (4)$$

where SNR is signal-to-noise ratio. CosmicFlows has shown that an

HI spectrum is considered adequate for estimating galaxy distance through the TFR if the error on W_{m50} is less or equal to 20 km s^{-1} . As seen in Figure 2 this threshold is confirmed once again by this study.

In summary for the three algorithms for W_{m50} : (1) SoFiA is automated but sometimes gives discrepant measurements for low SNR spectra (see Figure 1). It also has a dispersion of about 50 km s^{-1} , which is too high for Tully-Fisher purposes (Courtois et al. 2009). (2) The adopted CF algorithm is semi-automated, with a final inspection by eye of the fit. In some cases (six spectra, corresponding to about 1% of all spectra in the pilot survey), a fit was not possible. (3) The S16 algorithm requires a starting value for W_{m50} (that can be provided by SoFiA), but appears to provide a measurement which is within the 20 km s^{-1} error limit on W_{m50} that we impose for TFR studies. S16 is therefore used to complement CF measurements in cases where the latter fails.

Details of all the galaxies selected at 21 cm for this TF study are found in Appendix A.

2.3 Comparison with other velocity width measurements

TFR measurement and calibration is sensitive to random and systematic errors, as well as to catastrophic errors brought about by confusion or one-sided profiles. For these reasons, it is important to check our velocity widths against existing data. This is particularly important in order to check whether there are any systematics which may arise between single-dish and interferometer spectroscopic data. For example, missing flux in interferometer data may reduce the amount of extended flat-rotation curve gas in the reconstructed profile and decrease the velocity width measurement. Similarly, due to large single-dish beamwidths, HI detections may have wrong optical cross-identifications, typically wrongly identifying a host that is brighter and of larger mass than the correct identification.

Fortunately, there is a sufficient overlap with existing data to check consistency between pilot WALLABY and published single-dish velocity widths as compiled in the Extragalactic Distance Database (Courtois & Tully 2015). This comparison is shown in Figure 3 for the galaxies in common. There is no significant difference when comparing the WALLABY W_{mx} values with those measured from single-dish data, with most agreeing within the 20 km s^{-1} limit. The discrepant data comes from wrong width measurements from low S/N ratio Arecibo spectra and measurements of WALLABY spectra containing residual continuum from strong nearby sources outside the field and therefore not cleaned. This comparison is an excellent

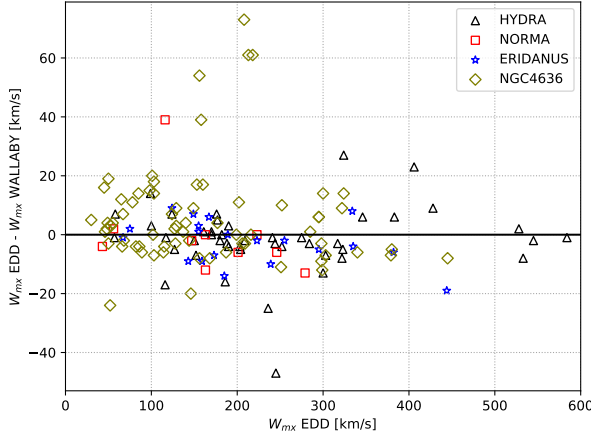


Figure 3. Comparison of the WALLABY pilot phase velocity widths presented in this article with single-dish data in the Extragalactic Distance Database (Courtois & Tully 2015). Widths are only compared where the internal error for W_{m50} in both datasets is less or equal to 20 km s^{-1} . Measurements mostly agree within the 20 km s^{-1} limit. The large offsets are either due to low SNR Arecibo spectra or due to noisy WALLABY spectra with residual baseline ripples due to residuals caused by strong radio continuum sources. The latter is more prominent in the NGC4636 field, which lies close to 3C273.

external robustness assessment of the capability of WALLABY to deliver satisfactory HI data to the community.

2.4 WISE Photometry

The *Wide-Field Survey Explorer* (WISE) satellite provides all-sky photometric observations in 4 mid-infrared bands, $W1 = 3.4\mu\text{m}$, $W2 = 4.6\mu\text{m}$, $W3 = 12.0\mu\text{m}$, $W4 = 22.8\mu\text{m}$ (Wright et al. 2010).

We initially tried to use data from the WISE all sky catalog GATOR web interface. When plotting the TFR we found that this instrumental profile-fit magnitudes were not appropriate for photometry of extended sources. As can be seen in Figure 4, the derived Tully-Fisher relation was totally unprobable.

Thus in this article, the photometric parameters are measured from the WISE observations using the photometric pipeline from Jarrett et al. (2013), where mosaics of each source are optimally constructed for resolved sources, carefully preserving the native angular resolution of WISE single frames (Jarrett et al. 2012). Source characterization includes size, shape, orientation, surface brightness and photometric measurements.

These measurements serve as the basis for derived physical parameters, including size, luminosity, stellar mass and star formation rate. The aggregate stellar mass is estimated using the $W1$ in-band luminosity and the $W1-W2$ colour (to account for the population-dependent mass-to-light ratio), as described in Cluver et al. (2014). The global star formation rate is estimated from the $W3$ and $W4$ spectral luminosities, after subtracting the stellar continuum, as detailed in Cluver et al. (2017); Jarrett et al. (2019).

The pipeline returns several types of apparent magnitude including, 1-sigma isophotal magnitudes, asymptotic magnitudes, and total radial-profile-modeled magnitudes. The Tully-Fisher relation is an empirical relation between maximum rotation velocity and total luminosity, i.e. total stellar mass of the galaxy. We therefore used the total extrapolated magnitude which encompasses the isophotal

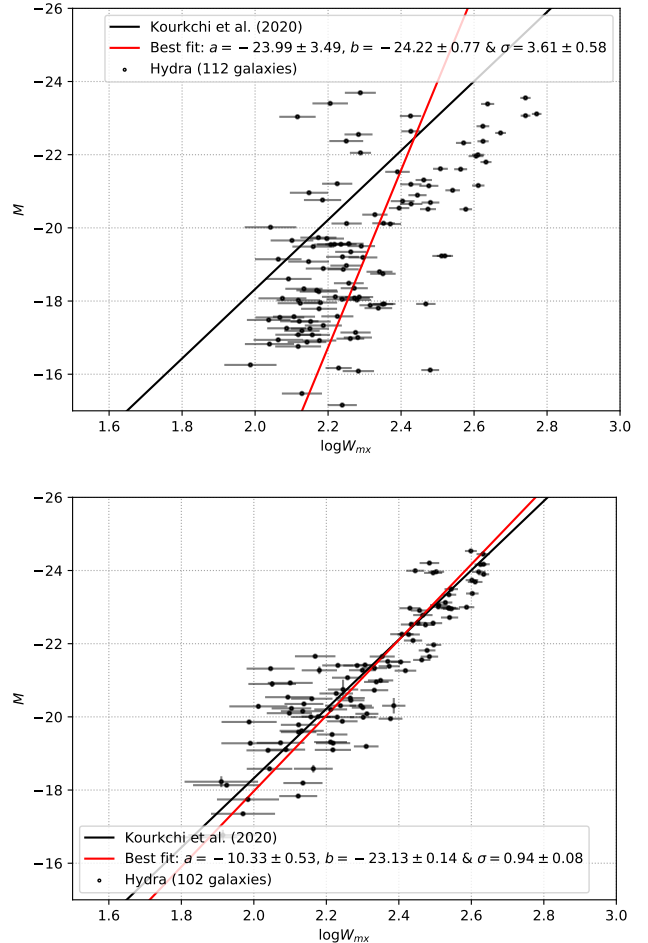


Figure 4. Comparison of TFR for Hydra using the public WISE Photometry (top-panel) and using our newly derived WISE Photometry. The rms deviations from the best fit line (red-line) decreases from 3.6 to 0.9 when using the new photometry. Furthermore, the best fit parameters are very close to the universal calibrated relation. The best fit parameters (red lines) are from the hyperfit package (Robotham & Obreschkow 2015) which uses errors in both axes.

measured magnitude plus extrapolation of the radial SB profile to 3 disk scale lengths for our analysis.

The second measured parameter that is needed for the TFR is the inclination which is extracted from the WISE observations. We used the measured axis ratio based on the $W1$ 3-sigma isophote to derive the inclination. We caution that the axis ratio and position angle are sensitive to the angular size of the galaxy due to the relatively large beam, $\text{FWHM} = 6''$, of the $W1$ imaging. Moreover, the near-infrared is sensitive to older stellar populations, and notably the bulge population, which tends to circularize the axis ratio and hence appear more face-on with inclination.

3 TULLY-FISHER DISTANCES

Measuring distances requires a redshift independent distance indicator which can be either primary indicator such as the Cepheid variable stars (Fernie 1969) or secondary indicator such as, the Tully-Fisher relation (Tully & Fisher 1977). In this paper, we will be adopting

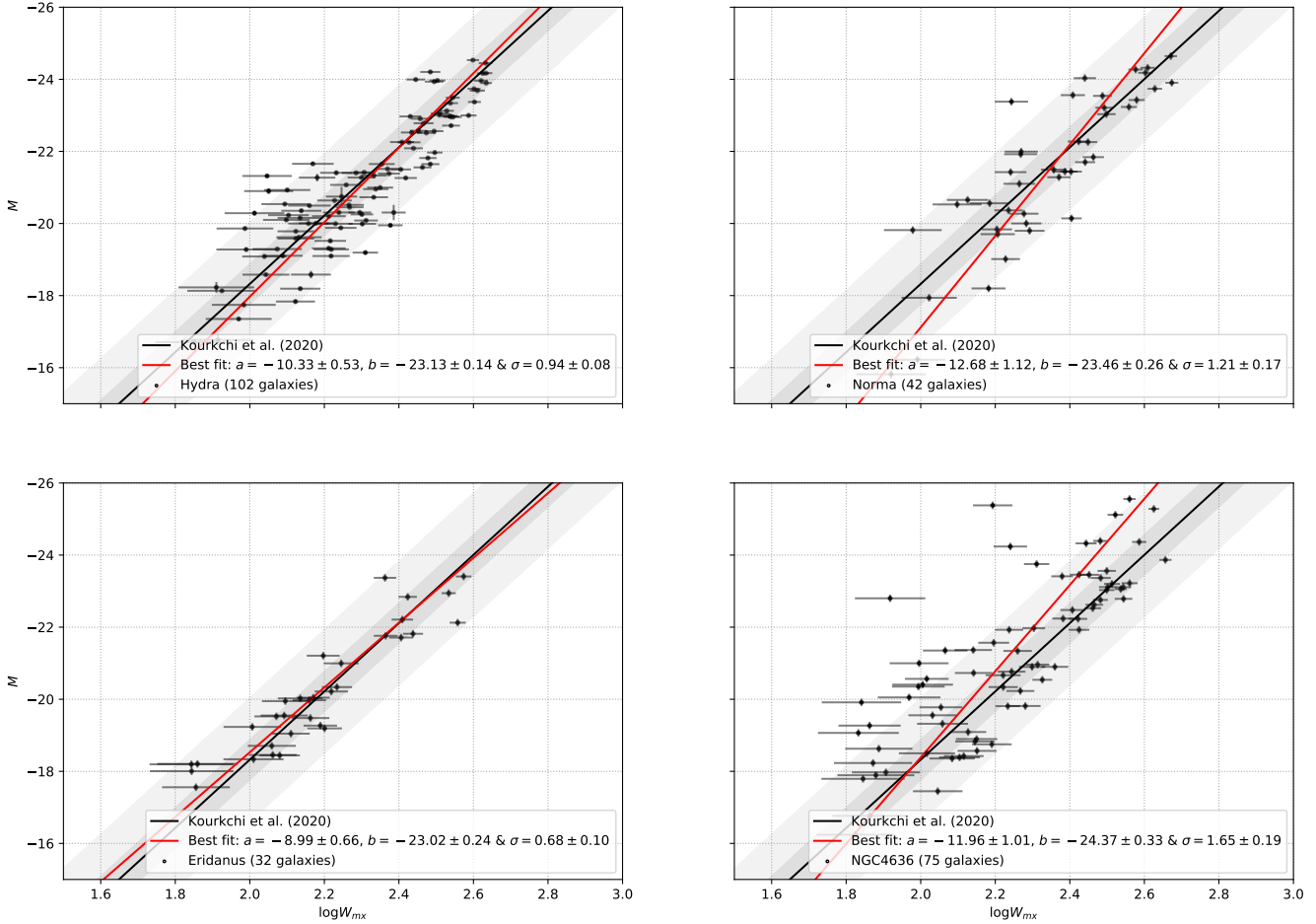


Figure 5. TFR for the four fields in the WISE $W1$ band. The solid black line is the calibrated TFR from Kourkchi et al. (2020a); the dark and light shaded areas correspond to $1-\sigma$ and $3-\sigma$ scatter around the TFR, respectively; the solid red line is the best fit model. The quantities derived with the Pilot survey are in good agreement with the WISE $W1$ TFR calibration in K20 in the Hydra, Norma and Eridanus fields. The high scatter in the NGC4636 field is due to the noisy spectra caused by residual radio continuum.

the Tully-Fisher relation as our workhorse to measure distances to spiral galaxies in the four WALLABY fields. As the name suggests, a secondary distance indicator such as the TFR should be calibrated first using a sample of spiral galaxies with known distances.

Kourkchi et al. (2020a, K20 hereafter) re-calibrated the TFR using optical u , g , r , i and z SDSS bands as well as infrared $W1$ and $W2$ WISE bands. We will use the WISE $W1$ calibrated relation as our standard tool in deriving the distances of galaxies in the WALLABY fields. Although the sample used to re-calibrated the TF is different from our WALLABY sample, parameters, methods and corrections should be as consistent as possible. In this section we will go through all parameters that we used to derive the distances for all four WALLABY fields and their associated corrections.

With the calibrated TFR in WISE $W1$ (K20) in hand, two sets of observations are required to derive TF distances: (A) spectroscopic observations (in our case HI 21-cm) from which we extract the galaxy rotational velocity; (B) photometric observations (in our case infrared imaging) from which we extract the apparent magnitude for each galaxy in our sample.

The first set of data is the WALLABY 21-cm spectra. The raw spectra were fitted using three different algorithms. The full pre-

sentation of this data set is in Section 2. To be consistent with the calibrated TFR from K20, we used the same method and corrections as CosmicFlows to derive the W_{mx} line width (i.e., see section 2.2). The only difference is that, while CosmicFlows visually measured inclinations, here we are using WISE $W1$ band photometric parameters (Section 2.4) to derive the inclination as:

$$\cos^2 i = \frac{(b/a)^2 - q_0^2}{1 - q_0^2} \quad (5)$$

where q_0 is the intrinsic axial ratio of the galaxy, $q_0 = 0.13$ for Sbc and Sc, and $q_0 = 0.2$ for other types (Giovanelli et al. 1997). We didn't make a search for the morphological type, so we used $q_0 = 0.2$ if $b/a > 0.2$ and $q_0 = 0.13$ if $b/a \leq 0.2$. Galaxies with axial ratio (b/a) greater or equal to 0.7 are excluded to avoid large corrections in the line width due to the inclination correction.

The heliocentric redshift can be measured from the WALLABY 21-cm spectra. Tully-Fisher distances are weakly dependent on redshifts through the k -correction. We furthermore use redshifts to visualize the data (e.g., Figures 5 and 8). However, redshift is a crucial parameter for the derivation of the peculiar velocity or the logarithmic distance ratio which is beyond the scope of this paper and will be

discussed in subsequent WALLABY papers. For the purpose of this paper, we first convert the heliocentric redshift z_{helio} to the CMB redshift z_{CMB} using,

$$z_{\text{CMB}} = \frac{1 + z_{\text{helio}}}{1 + z_{\text{Sun}}} - 1, \quad (6)$$

where z_{Sun} is the velocity of the sun with respect to the CMB in the direction of the galaxy being measured. It is calculated using the Planck dipole (Planck Collaboration et al. 2020). We derive the comoving distance $D(z_{\text{CMB}})$ in Mpc at redshift z_{CMB} using a flat ΛCDM with $H_0 = 75 \text{ km s}^{-1} \text{ Mpc}^{-1}$ and $\Omega_m = 0.27$ and convert this to luminosity distances using:

$$D_L = (1 + z_{\text{helio}})D(z_{\text{CMB}}). \quad (7)$$

The second set of data consists of photometric imaging from WISE $W1$. The full description of the data reduction process, from building mosaics to deriving the photometric parameters of interest, is given in section 2.4. The correction to apparent magnitudes is applied in the same manner as for the calibrated relation (K20):

$$m_{\text{cor}} = m_{\text{obs}} - A_{W1} - k_{W1} - I_{W1}, \quad (8)$$

where m_{cor} is the desired corrected magnitude, m_{obs} is the observed total magnitude, A_{W1} is the extinction correction due to dust from our own Galaxy (Schlegel et al. 1998), k_{W1} is the k -correction of the form $A_{W1}^k = -2.27z$ (Oke & Sandage 1968; Huang et al. 2007), and I_{W1} is the correction for internal extinction which were considered but neglected because they are small in $W1$ band. Sakai et al. (2000) parameterize them as $\gamma \log a/b$. If the effective wavelength of $W1$ is $3.4\mu\text{m}$, and the absorption in magnitudes is proportional to λ^{-1} , the maximum value is less than 0.1 mag for $\log w = 2.5$.

The absolute magnitude for each galaxy, for the purpose of visualizing the data only, was calculated as:

$$M = m_{\text{cor}} - 5 \log_{10}(D_L) - 25. \quad (9)$$

Figure 5 visualizes the three ingredients needed for the TFR: (A) the solid line denotes the calibrated TFR in WISE $W1$ and the associated 1- σ and 3- σ regions (shaded areas); (B) the velocity width $\log W_{\text{mx}}$, on the x -axis is the maximum rotational velocity derived from the WALLABY spectra (Section 2.2); (C) the absolute magnitude M , on the y -axis is derived from Equation 9. The TFR fit is performed using the hyperfit method (Robotham & Obreschkow 2015), allowing varying uncertainties in both axes.

We calculated the scatter about the TFR for the four WALLABY fields in Fig. 5. The rms for Hydra is 0.90 ± 0.08 mag, which is comparable to the value of 0.89 found by K20 for the same cluster. The rms scatter in the Norma field is 1.18 ± 0.17 mag which is slightly higher than most of the individual clusters in K20. The higher rms scatter in the TFR in Norma field is due to the strong dust extinction and stellar confusion which affects the photometric data reduction. The scatter about the TFR in Eridanus field is 0.58 ± 0.08 mag which is the smallest of all the four fields and is identical to the rms scatter of the final calibrated TFR from K20. The rms scatter about the TFR in the NGC4636 region is the highest at 1.61 ± 0.19 mag. The source of this scatter may be the noisy WALLABY spectra with baseline ripples due to residuals caused by strong radio continuum sources in the NGC4636 field (see Fig. 3).

Furthermore, source finding in the N4636 group was done in a different way from the other fields (Hydra, Norma and Eridanus). It was done by searching at the coordinates (RA, Dec, z) of previously catalogued galaxies, while the source finding for the other clusters

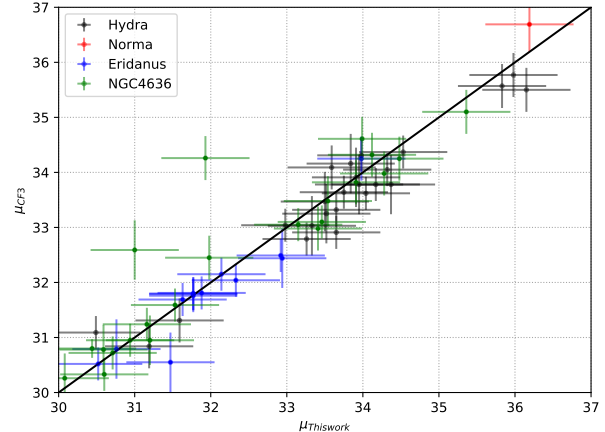


Figure 6. Comparison of the distance modulus measurements from the WALLABY pre-pilot survey (this work) vs. CosmicFlows-3 (Tully et al. 2016)

was done blindly. The master catalogue providing input coordinates for NGC4636 was a combination of SDSS, ALFALFA, HIPASS and 6dFGS. Moreover the northern tile of the NGC 4636 field consists of only a single footprint, as the other footprint had to be discarded due to data quality issues. Hence, the noise level in the northern half of the field is significantly higher than in all other fields.

With all parameters in hand, the absolute magnitude of each galaxy can be read off from the calibrated TFR given its maximum rotational velocity as:

$$M(W_{\text{mx}}) = -(20.36 \pm 0.07) - (9.47 \pm 0.14)(\log_{10} W_{\text{mx}} - 2.5) - 2.699, \quad (10)$$

where the TFR slope is (-9.47 ± 0.14) , the zero point is (-20.36 ± 0.07) , and the conversion of the AB to the Vega system is 2.699.

Using the apparent and absolute magnitude derived from equations 8 & 10, we can calculate the distance modulus as:

$$\mu = m_{\text{cor}} - M(W_{\text{mx}}). \quad (11)$$

Cross-matching with the CosmicFlows-3 (CF3) catalog (Tully et al. 2016) result in 24 source matches in Hydra, 1 in Norma, 13 in Eridanus, and 24 in the NGC4636 field. We compared our measurements for the distance modulus to the published ones from CF3. Figure 6 shows the comparison of the distance modulus from the four WALLABY fields with the ones from CF3. Figure 6 shows that our measurements appear to be systematically higher than the CF3 measurements. This can be due to the zero point offset calibration which is adjusted for the CF3 measurements but not for our WALLABY measurements. The zero point calibration will not be an issue for WALLABY measurements in the future, given the large sky-area which will allow it to easily be adjusted using more accurate measurements such as SN Ia.

The distribution of the measured TF distances in the four WALLABY fields are shown in Fig. 7. The WALLABY Hydra field includes background galaxies that do not belong to the Hydra cluster. The same applies to the Norma and Eridanus fields. Measuring distances to the Hydra, Norma, NGC 4636 and Eridanus clusters will therefore require restrictions on redshift.

Fortunately, there is a clear distinction in the redshift distribution between the galaxies in the cluster and the background galaxies in the

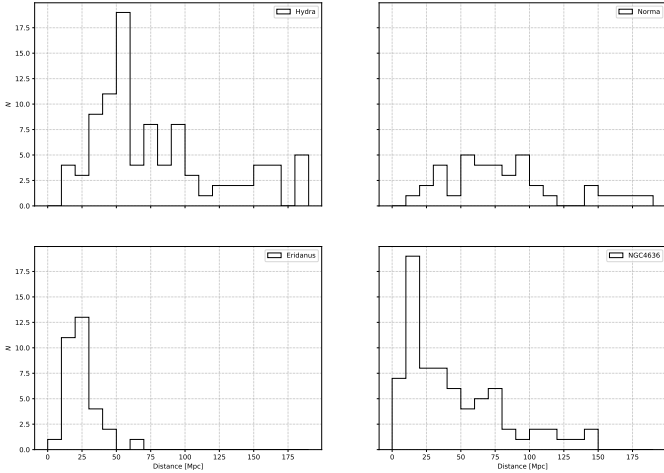


Figure 7. TFR distance distribution of galaxies in the four fields after extinction and k-corrections and the b/a cut < 0.7 using K20 calibration.

Hydra, Norma, and Eridanus fields. Figure 8 shows the redshift distribution in the four WALLABY fields. The dashed-red lines represent the distinction line between the cluster galaxies and the background ones. Using only galaxies with redshifts in the low-redshift side of the dashed-red lines, we measured the weighted average distance to Hydra, Norma, NGC 4636 and Eridanus to be 53.5 ± 2.5 , 69.4 ± 5.5 , 23.0 ± 2.1 and 21.5 ± 1.4 Mpc, respectively. In this study, the Norma distance refers to the eastern overdensity (which is part of the Norma supercluster). This distance may be slightly different from the cluster distance due to filament projection. In the next section a comparison with previous determinations of these distances will be made.

Peculiar velocities are the non-Hubble velocities induced gravitationally by large scale structure. For a Hubble Constant between 68 and 73 km/s/Mpc the peculiar velocities of the Hydra, Norma, NGC 4636 and Eridanus clusters lie in the range $(-320, -40)$, $(-730, -350)$, $(300, 430)$ and $(0, 110)$ km s $^{-1}$ respectively.

4 SPATIAL DISTRIBUTION OF GALAXIES IN THE PHASE 1 PILOT SURVEY

Figure 8 illustrates the variance in the redshift distribution between the WALLABY pilot survey fields and the presence of cluster foreground and background galaxies. It also shows that the pilot integration times allow us to reach a recessional velocity of 15,000 km s $^{-1}$, doubling what has been achieved by predecessor all-sky surveys reliant on single dish observations, such as 2MTF. These higher redshifts have so far only accessible using fundamental plane techniques – e.g. 6dFGS, which provides about 6,000 useful peculiar velocities. WALLABY is expected to deliver about 30,000-50,000 peculiar velocities.

4.1 Hydra and Norma clusters fields

The Hydra cluster has a mean redshift of 0.012 (Babyk & Vavilova 2013) and a velocity dispersion of 690 km s $^{-1}$ (Lima-Dias et al. 2021). Figure 8 shows the redshift distribution for Hydra cluster galaxies in our sample whereas Fig. 5 shows the TFR for these galaxies.

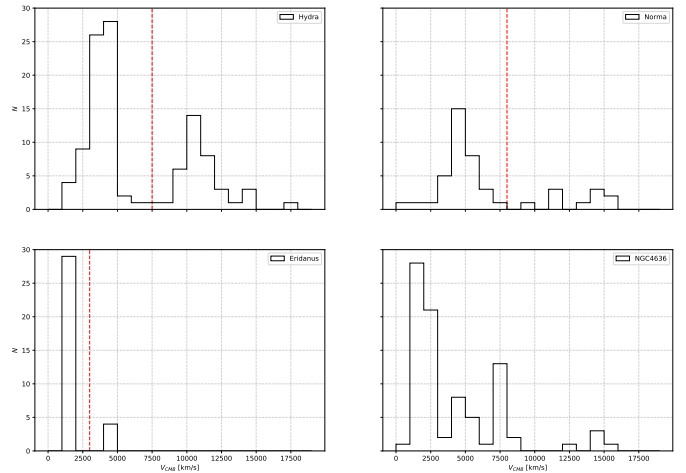


Figure 8. The redshift distribution (CMB frame) of all 614 galaxies in the Hydra, Norma, Eridanus and NGC4636 fields. The dashed-red lines in the Hydra, Norma and Eridanus plots represent the estimated division between the cluster and background galaxies. The WALLABY pilot integration time allows the detection of galaxies located at 15,000 km s $^{-1}$, around twice the distance limit of previous single dish surveys such as HIPASS.

Woudt et al. (2008) find a mean velocity of 4871 ± 54 km s $^{-1}$ for the Norma cluster and locate its centre at $(l, b) = (325.3^\circ, -7.2^\circ)$. They identify it as the richest cluster in the region of the Great Attractor. Mutabazi (2021), in a study of its fundamental plane, finds a small peculiar velocity. The WALLABY pilot survey field is centred on $(l, b) = (329.3^\circ, -10.4^\circ)$, i.e. 5.1° , respectively 6 Mpc from the cluster center. Nevertheless, there is clear overdensity of galaxies visible at the cluster redshift (Fig. 8).

A full 3D view of the Great Attractor region with the first CosmicFlows reconstruction of the local velocity field near Norma and Hydra clusters was presented by Courtois et al. (2012). Infall to the Norma cluster takes the form of a sharper distribution in redshift space than in real space (see Figure 9).

The positions of WALLABY galaxies within the Cosmic Web can be studied using the full matter (dark and luminous) density contrast field (usually noted δ) reconstructed from the CosmicFlows-3 Catalog of peculiar velocities (Graziani et al. 2019; Tully et al. 2019; Courtois et al. 2019; Pomarède et al. 2020). Figure 9 shows the redshift locations of galaxies of the Norma survey versus a real-space three-dimensional visualization of the overdensity field, restricted to a slice. The visualization is obtained by a combination of a ray-casting algorithm (Pomarède et al. 2017a) resulting in a smooth rendering of the δ overdensity field ranging from most underdense (deep blue colour) to most overdense (yellow), and a series of semi-transparent isosurface polygons resulting in a sharp materialization of the surfaces ranging from $\delta = 0$ (grey surface) to highly overdense ($\delta = 2.8$ in red). The grey surface hence marks the frontier between the underdense and the overdense Universe. The most noticeable feature in the distribution of WALLABY galaxies is their aggregation near the Norma cluster at $SGX \simeq -5000$ km s $^{-1}$, seen as a pronounced local maximum in the density contrast field (δ field). Between the Local Group and the Norma cluster, the field includes a section of the Local Void (Tully et al. 2019) and the termination of a filament connecting the Fornax cluster to the Norma cluster, as can better be seen from the interactive 3D visualization supplementing Figure 9

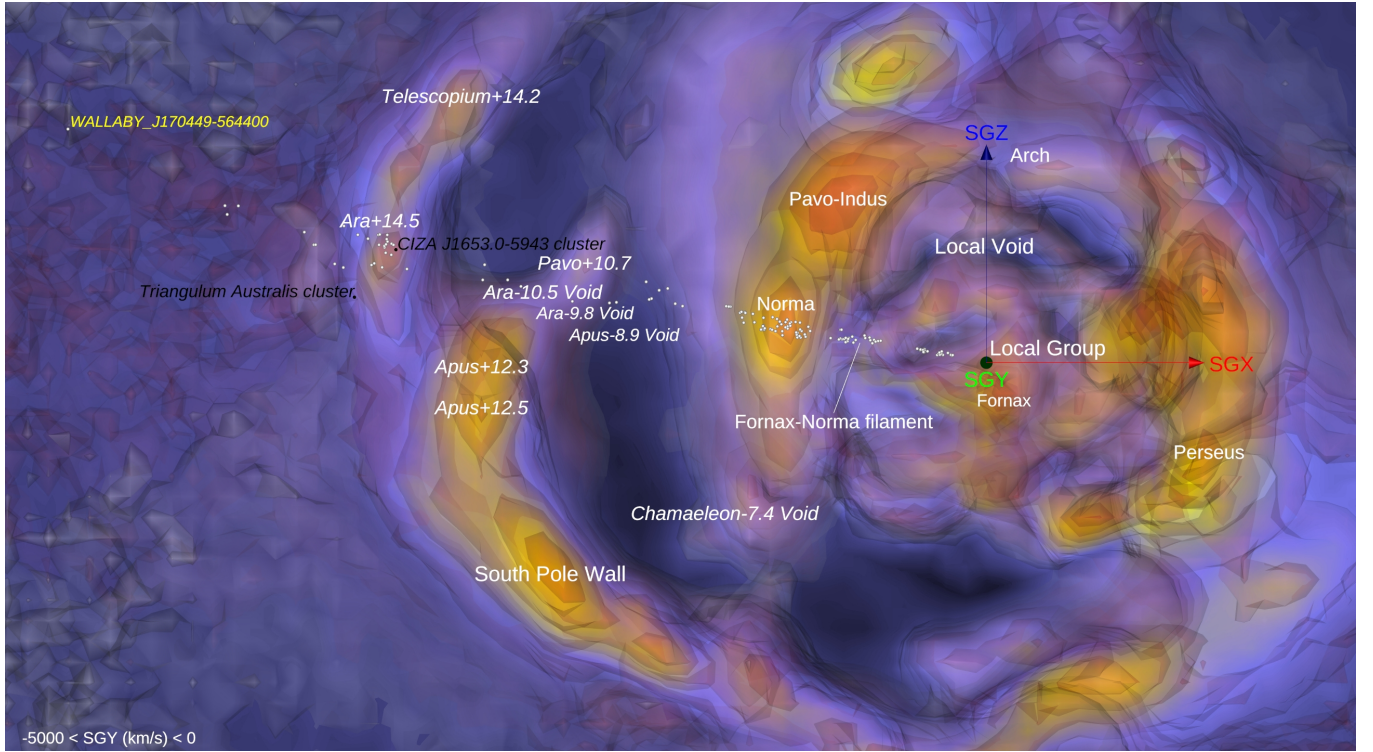


Figure 9. Map of the redshift positions of galaxies in the Norma field (white points) overlaid on the (coloured) density contrast field (δ) as reconstructed from the CosmicFlows-3 Catalog of peculiar velocities. Scale and orientation are provided by the red and blue 5000 km s^{-1} -long arrows emanating from our position and associated with the supergalactic coordinates SGX and SGY, respectively. A slice defined by $0 > \text{SGY} > -5000 \text{ km s}^{-1}$ is here seen from the negative SGY direction. This static view is complemented by an online [interactive 3D visualization of the Norma survey field](#) showing three levels of the overdensity δ , field. This tool can be used to better grasp how the field includes a series of voids and overdensities.

(see annotations 2 and 3). Beyond the Norma-Pavo-Indus filament (Fairall 1998; Courtois et al. 2013), the field includes the void separating this filament and the South Pole Wall (Pomarède et al. 2020). The map of Figure 9 indicates the location of local extrema of the over and under-density field δ , such as the Ara-10.5 Void and the Ara+14.5 overdensity, whose names include the name of the constellation in which they sit, followed by a ‘+’ for an overdensity or a ‘-’ for an underdensity, followed by their redshift in units of 1000 km s^{-1} , a convention established in Tully et al. (2019). An aggregation of WALLABY galaxies is found at the location of the Ara+14.5 knot of the Cosmic Web, that is nearly coincident with the CIZA J1653.0-5943 cluster (Ebeling et al. 2002). Beyond this most distant section of the South Pole Wall, the field presumably enters a new void, in regions where the CosmicFlows-3 reconstruction tends to a null field due lack of sufficient data. The most distant galaxy in the Norma field, located at redshift 0.073, is indicated on the map.

In Fig. 10 the distribution of the WALLABY galaxies in the Hydra field is plotted in a similar way on top of the CosmicFlows-3 cosmography. The density of WALLABY galaxies as a function of distance displays contrasting features: after displaying a handful of galaxies located in our vicinity at $\approx 900 \text{ km s}^{-1}$, no galaxies are detected in the void located in the foreground of the Hydra cluster. A major aggregation of objects is then seen at the crossing of the Hydra cluster, which is part of a high-density node in the Cosmic Web, as seen in the map of the CosmicFlows-3 density contrast. In the background of the Hydra cluster, the surveyed region includes a deep void (Hydra-7.4) where very few galaxies reside. In the background of this void, there

is an extended cloud of galaxies scattered throughout a wall located in Hydra at about $10,000 \text{ km s}^{-1}$, where local maxima in the density are found: Hydra+9.7, Hydra+9.9 and Antlia+8.8. After dropping as a function of distance, the number density of galaxy rises again at the most extreme distances, with WALLABY J104910-282305 being the most remote one at $\sim 23,000 \text{ km s}^{-1}$. This infall pattern of peculiar velocities leads to a higher overdensity in redshift space (Fig. 8) than in real space (Fig. 7).

4.2 The NGC 4636 cluster and Eridanus fields

The spatial distribution of the galaxies of the NGC 4636 survey is shown in Figure 11. The highest density in the field is at the crossing of the Virgo Strand (Courtois et al. 2013), a section of the Centaurus-Virgo filament that connects the Centaurus and Perseus nodes of the Cosmic Web through the Virgo cluster (Pomarède et al. 2017b), in which the NGC 4636 cluster is nested. Beyond the cluster, the field includes the outskirts of the void located between Virgo and the Great Wall (Gregory & Thompson 1978), and also includes part of the Centaurus-Coma filament (Pomarède et al. 2017b). The number of galaxies then rises at the intersection of the Great Wall (de Lapparent et al. 1986) near the Virgo+6.3 and Virgo+7.1 local maxima of the density contrast. In the background of the Great Wall, there is the trough and peak of Virgo-10.3 and Virgo+14.5.

Finally, the location of the galaxies of the Eridanus super group survey is presented in Figure 12. It shows that the galaxies are found near the Fornax node in the Cosmic Web, and distributed along

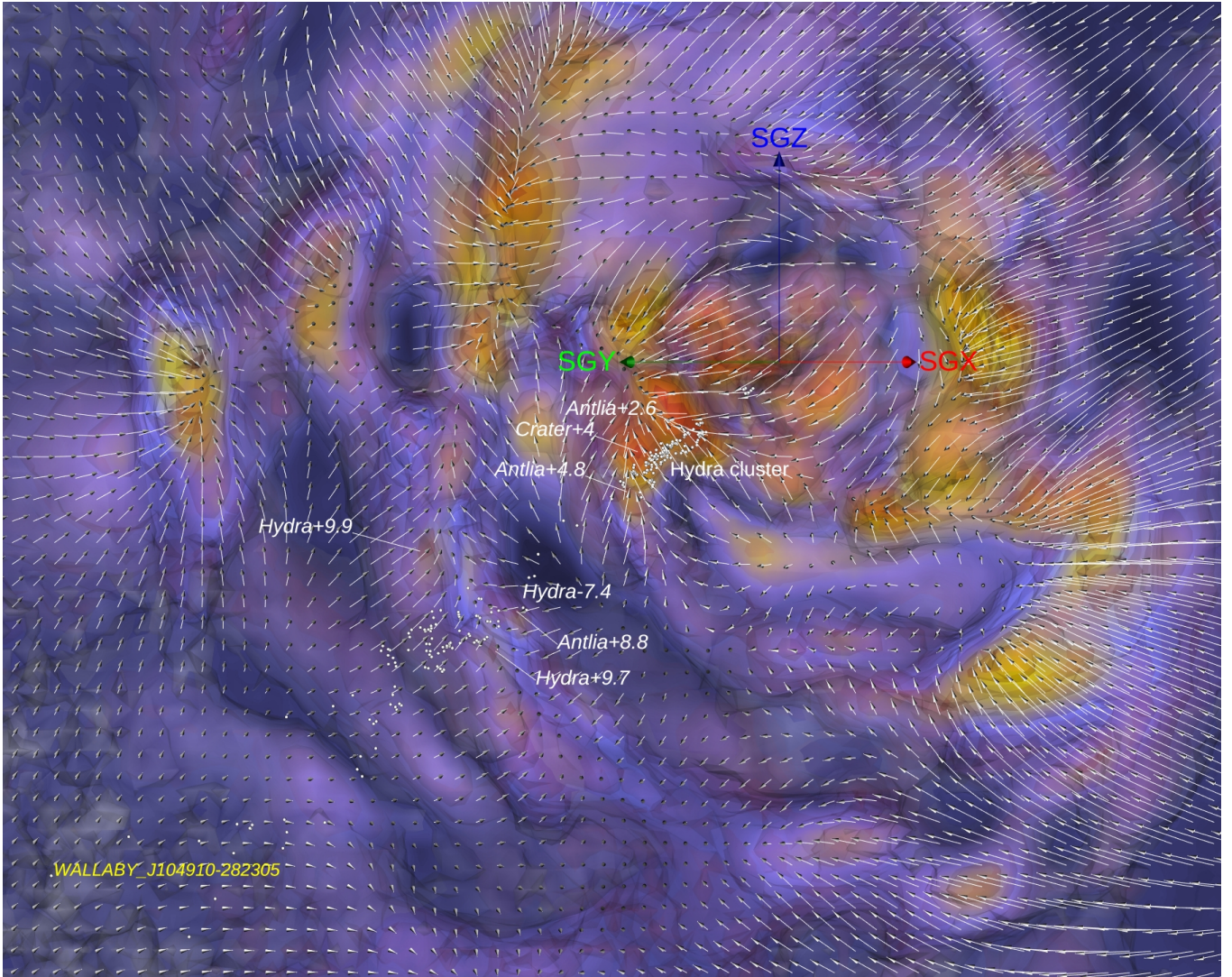


Figure 10. Map of the redshift positions of galaxies in the Hydra field (white points) overlaid on the (coloured) full matter (dark + luminous) density contrast δ , field and the peculiar (gravitational) velocity field (white arrows) as reconstructed from the CosmicFlows-3 Catalog. Scale and orientation are provided by the red, green and blue 5000 km s^{-1} -long arrows emanating from our position and associated with the three cardinal axes of the supergalactic coordinate system SGX, SGY, and SGZ, respectively. A slice of 5000 km s^{-1} -thickness centered on the plane defined by the supergalactic longitude of the Hydra cluster ($\text{SGL}=139.36^\circ$) is here seen face-on. This static view is complemented by an online [interactive 3D visualization of the Hydra survey beam](#) showing three levels of the overdensity δ , field. This tool can be used to better grasp how the field includes a series of voids and overdensities.

the density gradient seen in the transition toward the Sculptor Void located in the background (Pellegrini et al. 1990; Fairall 1998).

4.3 Discussion

The cosmographic maps presented in the previous section demonstrate that the WALLABY pilot survey fields probe a vast diversity of elements of the cosmic web: intersecting numerous features such as voids, filaments, walls, and the nodes which host the targeted clusters. The future inclusion of WALLABY-detected galaxies in the CosmicFlows collection will add useful data for cosmographical purposes. Of particular interest are the regions around the Hydra and Norma clusters and their roles in the dynamical structure and influence of the Great Attractor (Dressler et al. 1987; Woudt et al. 2008; Tully et al. 2014; Hoffman et al. 2017). WALLABY has the advan-

tage of being able to peer through the Galactic Plane, removing the so-called Zone of Avoidance which constrains all optical/IR surveys. Also of great interest are galaxies that reside in voids, which will provide improved constraints on the flows evacuating these underdense patches (Tully et al. 2008; Rizzi et al. 2017; Shaya et al. 2017). The most distant sections of the pilot fields, with velocities out to 22,000 km s^{-1} , will bring in new useful information on the architecture of the Cosmic Web in remote locations, thus providing better measurements of the large-scale gravitational field than currently available and potentially providing a definitive explanation for the amplitude of the CMB dipole.

In the vicinity of the Great Attractor, peculiar velocities for the Hydra and Norma fields show an infall pattern towards the respective clusters, i.e. positive peculiar velocities on the nearside of the clusters and negative on the far side. Beyond Hydra, positive velocities return

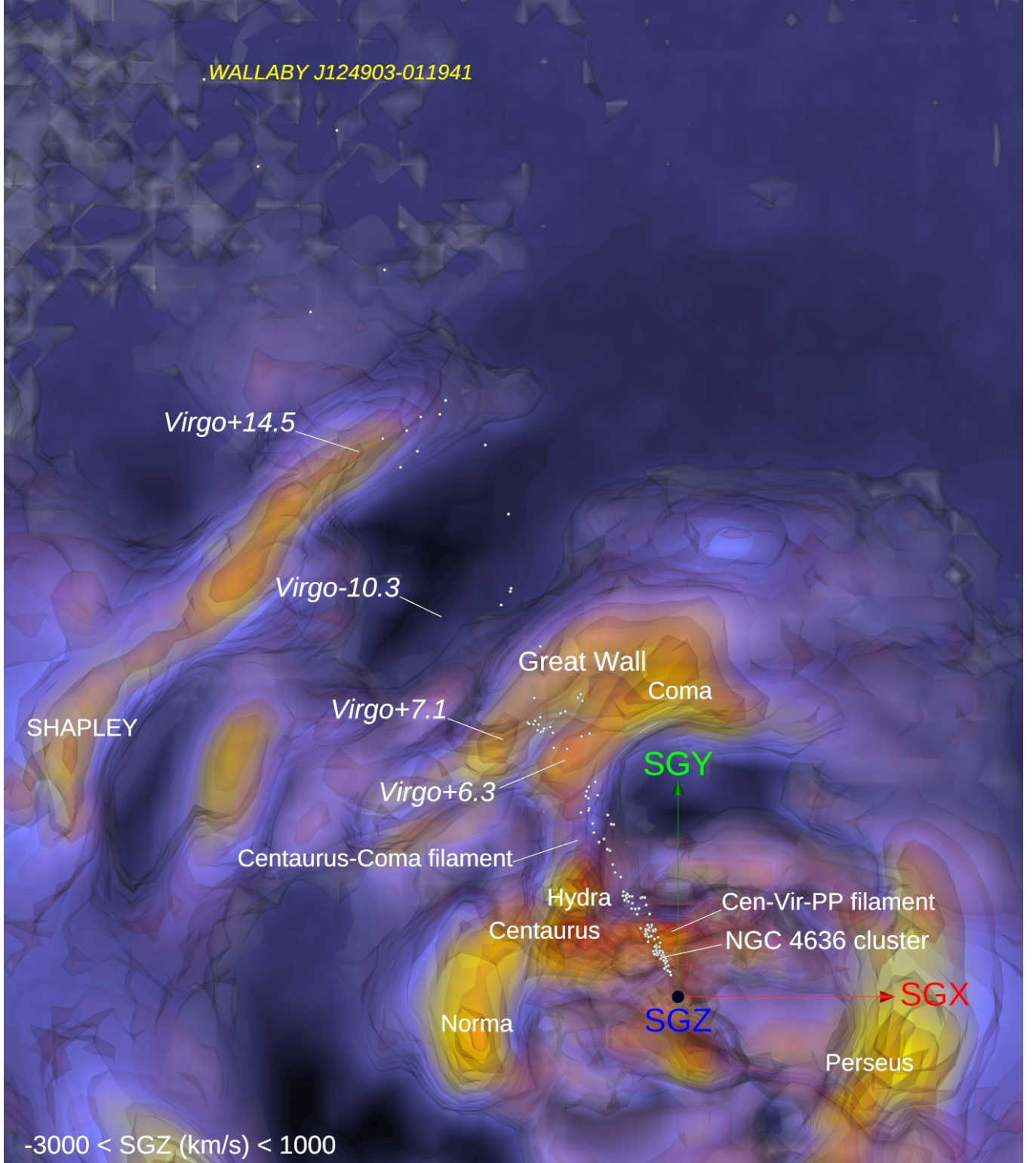


Figure 11. Map of the redshift positions of galaxies in the NGC 4636 field (white points) overlaid on the (coloured) density contrast δ , as reconstructed from the CosmicFlows-3 Catalog of peculiar velocities. Scale and orientation are provided by the red and green 5000 km s^{-1} -long arrows emanating from our position and associated with supergalactic coordinates SGX and SGY, respectively. A slice contained defined by $1000 > \text{SGZ} > -3000 \text{ km s}^{-1}$ is here seen from the positive SGZ direction. This static view is complemented by an online [interactive 3D visualization of the NGC 4636 survey field](#).

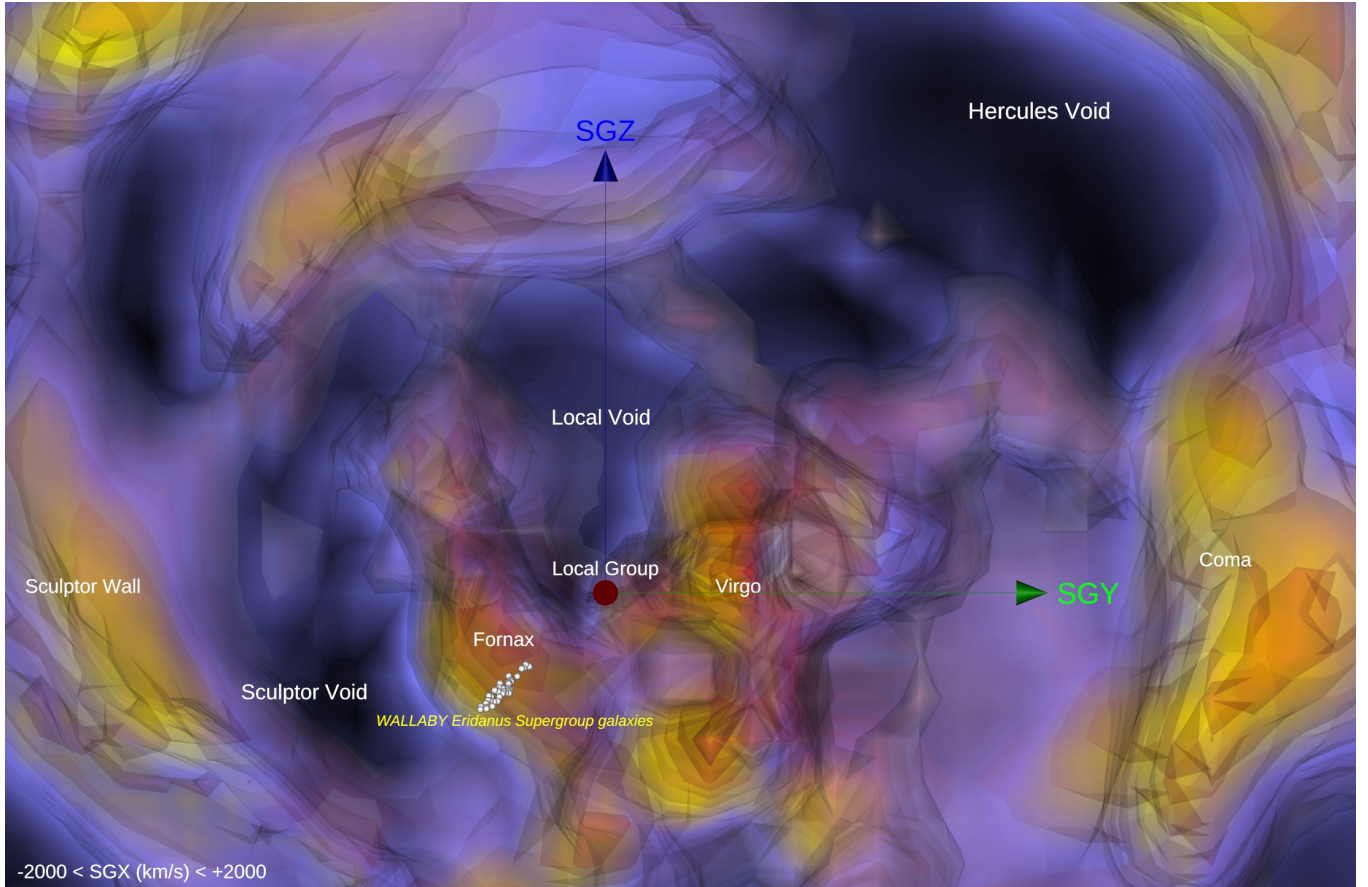


Figure 12. Map of the redshift positions of galaxies in the Eridanus super group (white points) overlaid on the (coloured) density contrast δ , as reconstructed from the CosmicFlows-3 Catalog of peculiar velocities. Scale and orientation are provided by green and blue 5000 km s^{-1} -long arrows emanating from our position and associated with supergalactic coordinates SGY and SGZ, respectively. A slice defined by $2000 > \text{SGX} > -2000 \text{ km s}^{-1}$ is here seen from the positive SGX direction. This static view is complemented by an online [interactive 3D visualization of the Eridanus super group survey](#).

as the galaxies come under the influence of the wall located at about $10,000 \text{ km s}^{-1} \approx 135 \text{ Mpc}$, seen in Figure 10 at the locations of the local maxima Hydra+9.7 and Hydra+9.9. The pattern observed in the peculiar velocities at $\sim 100 \text{ Mpc}$ is typical of an evacuation by the void located at 7400 km s^{-1} , labelled Hydra-7.4 in Figure 10, whereby galaxies located in the foreground of this void have negative velocities, while galaxies located in the background have positive velocities. The wealth of data represented by the WALLABY galaxies located along in this direction at these large distances will play an important role in mapping the structure currently hinted at by the CosmicFlows-3 reconstruction, in particular of the wall seen in Hydra at $10,000 \text{ km s}^{-1}$.

5 CONCLUSIONS

The Tully-Fisher distance of the Eridanus group is $21.5 \pm 1.4 \text{ Mpc}$, and its peculiar velocity for a Hubble constant of $68\text{--}73 \text{ km/s/Mpc}$ is small, between 0 and 110 km/sec . The NGC 4636 group is a complex structure within the Virgo cluster zero velocity surface, and its Tully-Fisher distance is $23.0 \pm 2.1 \text{ Mpc}$. Under the same assumptions its peculiar velocity is $300\text{--}430 \text{ km s}^{-1}$. The distance of the Hydra cluster is $53.5 \pm 2.5 \text{ Mpc}$. There is a substantial background group associated with the Shapely Supercluster. We measure a peculiar

velocity of $-320\text{--}40 \text{ km/s}^{-1}$ for the Hydra cluster, assuming $68 < H_0 < 73 \text{ km/s/Mpc}$. The Norma cluster is the most distant in the present sample at $69.4 \pm 5.5 \text{ Mpc}$. Its peculiar velocity is $-350\text{--}730 \text{ km s}^{-1}$ under the same assumptions.

This study also aims at testing the reliability, accuracy and dynamic range in distance able to be provided by Tully-Fisher distances for galaxies detected and parameterised in the pre-pilot and Phase 1 surveys of WALLABY. It is also a prediction for what the full survey will deliver. We find that :

- Measurements of galaxy velocity widths are in excellent agreement with those measured using previous single-dish observations, validating both the data quality and observational strategy of WALLABY.
- Even as close to the Zone of Avoidance as the Norma cluster, HI spectra provided by the SoFiA pipeline are excellent and extinction in the WISE W1 band is less than 0.1 mag. The combination of WALLABY and WISE W1 band observations will enable investigation of large number of accurate peculiar velocities of galaxies in the upcoming full WALLABY survey.
- The distribution of galaxies and kinematic pattern in the Hydra and Norma fields is one of infall to the cluster mass concentrations.
- The WALLABY pilot survey sensitivity and widefield capability will extend the investigation of peculiar velocities beyond what was

previously achieved with the single dish TFR method (e.g. twice the distance reached by 2MTF) and will improve on the accuracy of Fundamental Plane results (several times more galaxies than 6dFGS).

- WALLABY is a blind survey, rather than a targeted survey. Therefore many of the detections are of low S/N ratio. Further characterisation of the HI line width accuracy as a function of S/N ratio will need to be carried out with even larger datasets to better understand and exclude small biases.

ACKNOWLEDGEMENTS

The Australian SKA Pathfinder is part of the Australia Telescope National Facility which is managed by CSIRO. Operation of ASKAP is funded by the Australian Government with support from the National Collaborative Research Infrastructure Strategy. ASKAP uses the resources of the Pawsey Supercomputing Centre. Establishment of ASKAP, the Murchison Radio-astronomy Observatory and the Pawsey Supercomputing Centre are initiatives of the Australian Government, with support from the Government of Western Australia and the Science and Industry Endowment Fund. We acknowledge the Wajarri Yamatji people as the traditional owners of the Observatory site. Parts of this research were supported by the Australian Research Council Centre of Excellence for All Sky Astrophysics in 3 Dimensions (ASTRO 3D), through project number CE170100013. We would like to thank all our colleagues on the WALLABY team for helpful discussions. We have made use of NASA data products, including WISE and NED, and also NSF OIR Lab data products. We acknowledge the use of the HyperLeda database. HC is grateful to the Institut Universitaire de France and CNES for its support. KS, CH, and TD are supported by the Australian Government through the Australian Research Council's Laureate Fellowship funding scheme (project FL180100168). AD acknowledges financial support from the Project IDEXLYON at the University of Lyon under the Investments for the Future Program (ANR-16-IDEX-0005). AB acknowledges support from the Centre National d'Etudes Spatiales (CNES), France. DK acknowledges funding from the European Research Council (ERC) under the European Union's Horizon 2020 research and innovation programme (grant agreement no. 679627; project name FORNAX). RCKK is supported by the South African Research Chairs Initiative of the Department of Science and Technology and National Research Foundation. FB acknowledges funding from the European Research Council (ERC) under the European Union's Horizon 2020 research and innovation programme (grant agreement No.726384/Empire). Many thanks to Dmitry Makarov for helping us on the cross-identification with galaxy PGC names.

DATA AVAILABILITY

Distances, HI linewidths, and WISE magnitudes are available for the four fields in the online supplementary material. All other data from the parent catalogues will be shared on reasonable request to the corresponding author.

REFERENCES

- Aaronson M., Huchra J., Mould J., 1979, *ApJ*, **229**, 1
 Babyk I. V., Vavilova I. B., 2013, Odessa Astronomical Publications, **26**, 175
 Cluver M. E., et al., 2014, *ApJ*, **782**, 90
 Cluver M. E., Jarrett T. H., Dale D. A., Smith J. D. T., August T., Brown M. J. I., 2017, *ApJ*, **850**, 68
 Courtois H. M., Tully R. B., 2015, *MNRAS*, **447**, 1531
 Courtois H. M., Tully R. B., Fisher J. R., Bonhomme N., Zavodny M., Barnes A., 2009, *AJ*, **138**, 1938
 Courtois H. M., Tully R. B., Makarov D. I., Mitronova S., Koribalski B., Karachentsev I. D., Fisher J. R., 2011a, *MNRAS*, **414**, 2005
 Courtois H. M., Tully R. B., Héraudeau P., 2011b, *MNRAS*, **415**, 1935
 Courtois H. M., Hoffman Y., Tully R. B., Gottlöber S., 2012, *ApJ*, **744**, 43
 Courtois H. M., Pomarède D., Tully R. B., Hoffman Y., Courtois D., 2013, *AJ*, **146**, 69
 Courtois H. M., Kraan-Korteweg R. C., Dupuy A., Graziani R., Libeskind N. I., 2019, *MNRAS*, **490**, L57
 Dressler A., Faber S. M., Burstein D., Davies R. L., Lynden-Bell D., Terlevich R. J., Wegner G., 1987, *ApJ*, **313**, L37
 Ebeling H., Mullis C. R., Tully R. B., 2002, *ApJ*, **580**, 774
 Fairall A. P., 1998, Large-scale structures in the universe / Anthony P. Fairall. New York : Wiley, 1998.. Wiley-Praxis series in astronomy and astrophysics
 Fernie J. D., 1969, *PASP*, **81**, 707
 For B. Q., et al., 2021, *MNRAS*, **507**, 2300
 Giovanelli R., Haynes M. P., Herter T., Vogt N. P., da Costa L. N., Freudling W., Salzer J. J., Wegner G., 1997, *AJ*, **113**, 53
 Graziani R., Courtois H. M., Lavaux G., Hoffman Y., Tully R. B., Copin Y., Pomarède D., 2019, *MNRAS*, **488**, 5438
 Gregory S. A., Thompson L. A., 1978, *ApJ*, **222**, 784
 Haynes M. P., et al., 2018, *ApJ*, **861**, 49
 Hoffman Y., Courtois H. M., Tully R. B., 2015, *MNRAS*, **449**, 4494
 Hoffman Y., Pomarède D., Tully R. B., Courtois H. M., 2017, *Nature Astronomy*, **1**, 0036
 Hong T., et al., 2019, *MNRAS*, **487**, 2061
 Hotan A. W., et al., 2021, *Publ. Astron. Soc. Australia*, **38**, e009
 Huang J. S., et al., 2007, *ApJ*, **664**, 840
 Jarrett T. H., et al., 2012, *The Astronomical Journal*, **144**, 68
 Jarrett T. H., et al., 2013, *AJ*, **145**, 6
 Jarrett T. H., Cluver M. E., Brown M. J. I., Dale D. A., Tsai C. W., Masci F., 2019, *ApJS*, **245**, 25
 Koribalski B. S., et al., 2004, *AJ*, **128**, 16
 Koribalski B. S., et al., 2020, *Ap&SS*, **365**, 118
 Kourkchi E., Tully R. B., Neill J. D., Seibert M., Courtois H. M., Dupuy A. r., 2020a, *ApJ*, **884**, 82
 Kourkchi E., et al., 2020b, *ApJ*, **902**, 145
 Lagattuta D. J., Mould J. R., Staveley-Smith L., Hong T., Springob C. M., Masters K. L., Koribalski B. S., Jones D. H., 2013, *ApJ*, **771**, 88
 Lima-Dias C., et al., 2021, *MNRAS*, **500**, 1323
 Meyer M. J., et al., 2004, *MNRAS*, **350**, 1195
 Mould J., 2020, *Frontiers in Astronomy and Space Sciences*, **7**, 21
 Mutabazi T., 2021, *ApJ*, **911**, 16
 Neill J. D., Seibert M., Tully R. B., Courtois H., Sorce J. G., Jarrett T. H., Scowcroft V., Masci F. J., 2014, *ApJ*, **792**, 129
 Oke J. B., Sandage A., 1968, *ApJ*, **154**, 21
 Pellegrini P. S., da Costa L. N., Huchra J. P., Latham D. W., Willmer C. N. A., 1990, *AJ*, **99**, 751
 Peterson E. R., et al., 2021, arXiv e-prints, p. arXiv:2110.03487
 Planck Collaboration et al., 2020, *A&A*, **641**, A1
 Pomarède D., Courtois H. M., Hoffman Y., Tully R. B., 2017a, *PASP*, **129**, 058002
 Pomarède D., Hoffman Y., Courtois H. M., Tully R. B., 2017b, *ApJ*, **845**, 55
 Pomarède D., Tully R. B., Graziani R., Courtois H. M., Hoffman Y., Lezmy J., 2020, *ApJ*, **897**, 133
 Rizzi L., Tully R. B., Shaya E. J., Kourkchi E., Karachentsev I. D., 2017, *ApJ*, **835**, 78
 Robotham A. S. G., Obreschkow D., 2015, *Publ. Astron. Soc. Australia*, **32**, e033
 Said K., Kraan-Korteweg R. C., Staveley-Smith L., Williams W. L., Jarrett T. H., Springob C. M., 2016, *MNRAS*, **457**, 2366
 Said K., Colless M., Magoulas C., Lucey J. R., Hudson M. J., 2020, *MNRAS*, **497**, 1275
 Sakai S., et al., 2000, *ApJ*, **529**, 698
 Schlegel D. J., Finkbeiner D. P., Davis M., 1998, *ApJ*, **500**, 525

- Serra P., et al., 2015, [MNRAS](#), **448**, 1922
 Shaya E. J., Tully R. B., Hoffman Y., Pomarède D., 2017, [ApJ](#), **850**, 207
 Sorce J. G., et al., 2013, [ApJ](#), **765**, 94
 Springel V., et al., 2018, [MNRAS](#), **475**, 676
 Thévenot M., Cornen C., Goodwin B. L., Macmillan C., Stenner A. G., Téglás
 B., 2020, [Research Notes of the American Astronomical Society](#), **4**, 159
 Tully R. B., Fisher J. R., 1977, [A&A](#), **54**, 661
 Tully R. B., Fouqué P., 1985, [ApJS](#), **58**, 67
 Tully R. B., Shaya E. J., Karachentsev I. D., Courtois H. M., Kocevski D. D.,
 Rizzi L., Peel A., 2008, [ApJ](#), **676**, 184
 Tully R. B., Courtois H., Hoffman Y., Pomarède D., 2014, [Nature](#), **513**, 71
 Tully R. B., Courtois H. M., Sorce J. G., 2016, [AJ](#), **152**, 50
 Tully R. B., Pomarède D., Graziani R., Courtois H. M., Hoffman Y., Shaya
 E. J., 2019, [ApJ](#), **880**, 24
 Wang J., et al., 2021, [ApJ](#), **915**, 70
 Westmeier T., et al., 2021, [MNRAS](#), **506**, 3962
 Wong O. I., et al., 2021, [MNRAS](#), **507**, 2905
 Woudt P. A., Kraan-Korteweg R. C., Lucey J., Fairall A. P., Moore S. A. W.,
 2008, [MNRAS](#), **383**, 445
 Wright E. L., et al., 2010, [AJ](#), **140**, 1868
 de Lapparent V., Geller M. J., Huchra J. P., 1986, [ApJ](#), **302**, L1

APPENDIX A: DATA

The 21cm HI, WISE photometry, and TF distances catalog and plots of the HI spectra are available electronically. Tables in Appendix A present four catalogs of Hydra, Norma, Eridanus, and NGC4636. The parameters listed in the catalogs are:

Column (1) - WALLABY ID as reported in the WALLABY Pilot Survey data release (Westmeier et al., in prep.).

Columns (2) - Principal Galaxies Catalogue number (PGC)

Columns (3 and 4) - Right Ascension (RA) and Declination (Dec.) in the J2000.0 epoch of the fitted position in WALLABY.

Columns (5) - WISE W1 total magnitude after galactic extinction and k corrections.

Column (6) - Inclination calculated from WISE (b/a) as in equation 5.

Column (7) - Linewidths corrected for inclination.

Column (8) - CMB redshifts.

Column (9) - Tully-Fisher luminosity distances in Mpc.

Column (10 and 11) - Distance modulus and associated error.

Table A1: Hydra HI data from WALLABY phase 1 pilot survey.

| Name | PGC | RA | DEC | $W1_{tot}$ | i | W_{mx} | z_{cmb} | d_L | μ | e_μ |
|----------------|--------|----------|----------|------------|-----|----------|-----------|-------|-------|---------|
| J100342-270137 | 29166 | 150.9256 | -27.0271 | 10.73 | 79 | 185 | 0.004302 | 20.8 | 31.59 | 0.58 |
| J100351-273417 | 29179 | 150.9662 | -27.5715 | 8.95 | 51 | 422 | 0.010432 | 43.6 | 33.2 | 0.58 |
| J100426-282638 | 29216 | 151.1091 | -28.4442 | 9.97 | 73 | 203 | 0.00472 | 17.3 | 31.19 | 0.58 |
| J100640-273917 | 29378 | 151.667 | -27.6549 | 12.97 | 63 | 224 | 0.015361 | 83.3 | 34.6 | 0.58 |
| J100808-260942 | 29470 | 152.0353 | -26.1618 | 13.53 | 57 | 133 | 0.01142 | 40.3 | 33.03 | 0.58 |
| J100830-262140 | 768685 | 152.1256 | -26.3611 | 14.64 | 76 | 119 | 0.015122 | 54.0 | 33.66 | 0.58 |
| J100939-290112 | 154738 | 152.4128 | -29.0202 | 12.5 | 48 | 279 | 0.048043 | 101.9 | 35.04 | 0.58 |
| J101025-275214 | 748738 | 152.6054 | -27.8708 | 13.26 | 69 | 133 | 0.0092 | 35.5 | 32.75 | 0.58 |
| J101208-252000 | 154861 | 153.0362 | -25.3335 | 12.23 | 58 | 305 | 0.046845 | 106.9 | 35.14 | 0.58 |
| J101221-254604 | 29719 | 153.0904 | -25.7678 | 11.5 | 61 | 430 | 0.033304 | 146.4 | 35.83 | 0.58 |
| J101247-275028 | 29743 | 153.1998 | -27.8413 | 9.5 | 76 | 350 | 0.009848 | 39.4 | 32.98 | 0.58 |
| J101247-291053 | 732369 | 153.1962 | -29.1815 | 13.33 | 62 | 267 | 0.03197 | 138.1 | 35.7 | 0.58 |
| J101348-273147 | 29821 | 153.4516 | -27.5299 | 13.47 | 58 | 164 | 0.009818 | 58.4 | 33.83 | 0.58 |
| J101357-262550 | | 153.4904 | -26.4308 | 15.42 | 53 | 103 | 0.033823 | 59.3 | 33.87 | 0.58 |
| J101359-253824 | 29836 | 153.4964 | -25.64 | 13.3 | 71 | 205 | 0.011775 | 82.2 | 34.58 | 0.58 |
| J101359-274538 | | 153.4978 | -27.7607 | 16.25 | 74 | 71 | 0.009696 | 42.8 | 33.15 | 0.59 |

| | | | | | | | | | | |
|----------------|---------|----------|----------|-------|----|-----|----------|-------|-------|------|
| J101438-272431 | 29888 | 153.661 | -27.4087 | 10.91 | 54 | 386 | 0.014965 | 90.9 | 34.79 | 0.58 |
| J101441-285221 | 29892 | 153.6744 | -28.8726 | 7.48 | 72 | 312 | 0.004796 | 12.5 | 30.49 | 0.58 |
| J101448-285723 | 29903 | 153.7006 | -28.9565 | 10.55 | 73 | 401 | 0.015094 | 82.7 | 34.59 | 0.58 |
| J101526-264259 | 764730 | 153.8614 | -26.7166 | 13.91 | 48 | 301 | 0.03413 | 225.2 | 36.76 | 0.58 |
| J101531-292423 | 29945 | 153.8793 | -29.4066 | 12.44 | 66 | 338 | 0.031731 | 142.5 | 35.77 | 0.58 |
| J101537-272427 | | 153.9057 | -27.4078 | 15.6 | 49 | 96 | 0.01157 | 56.8 | 33.77 | 0.58 |
| J101632-291258 | | 154.1373 | -29.2163 | 13.19 | 76 | 176 | 0.015144 | 58.6 | 33.84 | 0.64 |
| J101756-285557 | | 154.4866 | -28.9325 | 14.54 | 68 | 171 | 0.037695 | 103.1 | 35.07 | 0.58 |
| J101834-281550 | 3753792 | 154.6456 | -28.264 | 14.92 | 48 | 152 | 0.041946 | 97.9 | 34.95 | 0.59 |
| J101920-264135 | 30161 | 154.8353 | -26.6931 | 12.34 | 57 | 319 | 0.044142 | 121.7 | 35.43 | 0.58 |
| J101927-264159 | 764945 | 154.8662 | -26.6999 | 14.36 | 50 | 110 | 0.00965 | 41.7 | 33.1 | 0.58 |
| J102017-253913 | 30216 | 155.0743 | -25.6538 | 13.53 | 52 | 150 | 0.012647 | 50.9 | 33.54 | 0.58 |
| J102019-285220 | 30218 | 155.0828 | -28.8722 | 11.16 | 77 | 429 | 0.032372 | 124.6 | 35.48 | 0.58 |
| J102023-253050 | | 155.0966 | -25.514 | 15.61 | 58 | 133 | 0.012113 | 104.3 | 35.09 | 0.58 |
| J102030-260951 | 30234 | 155.1281 | -26.1642 | 12.93 | 49 | 417 | 0.057252 | 266.3 | 37.13 | 0.58 |
| J102100-273339 | 753130 | 155.2535 | -27.5608 | 14.25 | 56 | 254 | 0.034427 | 191.3 | 36.41 | 0.58 |
| J102115-250342 | 783072 | 155.3137 | -25.0618 | 13.75 | 53 | 313 | 0.033934 | 226.2 | 36.77 | 0.58 |
| J102233-294017 | 726509 | 155.6378 | -29.6715 | 15.23 | 48 | 200 | 0.027189 | 192.0 | 36.42 | 0.58 |
| J102328-253424 | 777390 | 155.8685 | -25.5736 | 12.44 | 69 | 400 | 0.0417 | 196.1 | 36.46 | 0.58 |
| J102338-264531 | 764220 | 155.9116 | -26.7589 | 14.28 | 54 | 291 | 0.035818 | 250.3 | 36.99 | 0.58 |
| J102416-270241 | 760541 | 156.0683 | -27.0448 | 14.57 | 47 | 262 | 0.03579 | 235.2 | 36.86 | 0.58 |
| J102430-290904 | 732726 | 156.1259 | -29.1511 | 13.7 | 55 | 144 | 0.013634 | 50.6 | 33.52 | 0.58 |
| J102439-274841 | 749549 | 156.1626 | -27.8117 | 15.43 | 50 | 137 | 0.013157 | 101.9 | 35.04 | 0.58 |
| J102600-280334 | | 156.5018 | -28.0597 | 15.64 | 55 | 173 | 0.037564 | 175.9 | 36.23 | 0.58 |
| J102621-291150 | 732211 | 156.5886 | -29.1973 | 13.81 | 62 | 97 | 0.013451 | 25.3 | 32.01 | 0.58 |
| J102637-264142 | 764986 | 156.6545 | -26.6952 | 14.72 | 58 | 112 | 0.032546 | 50.8 | 33.53 | 0.59 |
| J102643-261256 | 770222 | 156.6797 | -26.2157 | 12.78 | 52 | 346 | 0.034396 | 174.2 | 36.2 | 0.58 |
| J102747-283425 | | 156.9461 | -28.5738 | 15.69 | 49 | 238 | 0.032729 | 328.3 | 37.58 | 0.58 |
| J102818-255446 | 773700 | 157.0764 | -25.9129 | 16.39 | 52 | 93 | 0.013865 | 76.9 | 34.43 | 0.58 |
| J102934-261937 | 30912 | 157.3949 | -26.3271 | 12.85 | 47 | 218 | 0.014271 | 74.9 | 34.37 | 0.58 |
| J103002-284116 | 738653 | 157.5091 | -28.688 | 13.21 | 61 | 124 | 0.013943 | 30.6 | 32.43 | 0.58 |
| J103015-270743 | 759425 | 157.5651 | -27.1287 | 14.61 | 69 | 215 | 0.037491 | 164.8 | 36.09 | 0.58 |
| J103114-295837 | 722930 | 157.809 | -29.9771 | 14.84 | 59 | 109 | 0.015115 | 51.0 | 33.54 | 0.58 |
| J103139-273049 | 753808 | 157.9143 | -27.5138 | 14.51 | 51 | 165 | 0.013058 | 95.5 | 34.9 | 0.58 |
| J103141-300815 | 720959 | 157.921 | -30.1377 | 15.09 | 63 | 98 | 0.018491 | 46.3 | 33.33 | 0.58 |
| J103240-282058 | 742765 | 158.169 | -28.3495 | 12.73 | 71 | 181 | 0.014228 | 50.1 | 33.5 | 0.58 |
| J103241-273137 | 31149 | 158.1721 | -27.5271 | 12.09 | 71 | 148 | 0.013911 | 25.3 | 32.02 | 0.58 |
| J103257-250937 | 782023 | 158.2381 | -25.1609 | 14.79 | 62 | 243 | 0.025659 | 226.1 | 36.77 | 0.62 |
| J103258-274013 | 31171 | 158.2426 | -27.6711 | 13.12 | 71 | 127 | 0.011609 | 30.6 | 32.43 | 0.58 |
| J103348-271429 | 757813 | 158.452 | -27.2417 | 13.17 | 56 | 347 | 0.036555 | 209.4 | 36.6 | 0.58 |
| J103353-274945 | 31238 | 158.4748 | -27.8291 | 12.36 | 60 | 215 | 0.010323 | 58.5 | 33.84 | 0.58 |
| J103359-301003 | 31242 | 158.4966 | -30.1677 | 9.87 | 79 | 408 | 0.012775 | 62.5 | 33.98 | 0.58 |
| J103420-265408 | 92288 | 158.5865 | -26.9023 | 14.08 | 79 | 135 | 0.013623 | 53.8 | 33.66 | 0.58 |
| J103502-293019 | 728536 | 158.7604 | -29.5062 | 12.38 | 50 | 111 | 0.013626 | 16.9 | 31.15 | 0.58 |
| J103507-275923 | 31334 | 158.783 | -27.9905 | 12.22 | 74 | 169 | 0.009264 | 34.6 | 32.69 | 0.58 |
| J103521-274137 | 31355 | 158.8391 | -27.6938 | 13.31 | 76 | 175 | 0.010796 | 61.6 | 33.95 | 0.58 |
| J103547-290131 | 31390 | 158.9463 | -29.0252 | 13.15 | 50 | 312 | 0.033811 | 170.2 | 36.15 | 0.58 |
| J103609-244856 | 31415 | 159.0412 | -24.8154 | 13.17 | 54 | 84 | 0.004545 | 14.3 | 30.78 | 0.58 |
| J103645-281010 | 744989 | 159.1902 | -28.1698 | 13.36 | 49 | 163 | 0.012783 | 54.7 | 33.69 | 0.58 |
| J103646-293253 | 31484 | 159.196 | -29.5482 | 13.3 | 51 | 197 | 0.013046 | 76.5 | 34.42 | 0.58 |
| J103650-270902 | 31490 | 159.2096 | -27.1485 | 13.22 | 68 | 293 | 0.038595 | 155.7 | 35.96 | 0.58 |
| J103651-260227 | 31491 | 159.2131 | -26.0412 | 13.62 | 50 | 204 | 0.009072 | 94.5 | 34.88 | 0.58 |
| J103653-270311 | 31494 | 159.2211 | -27.0532 | 12.08 | 55 | 234 | 0.012999 | 60.4 | 33.91 | 0.58 |
| J103655-265412 | 762452 | 159.233 | -26.9029 | 13.17 | 64 | 200 | 0.011978 | 73.7 | 34.34 | 0.58 |
| J103701-284018 | 738882 | 159.2551 | -28.6725 | 14.32 | 65 | 236 | 0.033688 | 172.0 | 36.18 | 0.58 |
| J103704-252038 | 31514 | 159.2683 | -25.3441 | 12.41 | 77 | 199 | 0.013539 | 51.8 | 33.57 | 0.58 |
| J103737-261641 | 31574 | 159.4074 | -26.2776 | 10.73 | 53 | 323 | 0.01386 | 59.6 | 33.88 | 0.58 |
| J103803-281007 | 31602 | 159.5132 | -28.1688 | 14.22 | 73 | 305 | 0.036341 | 267.0 | 37.13 | 0.58 |
| J103809-260453 | 31612 | 159.5414 | -26.0815 | 13.11 | 73 | 145 | 0.013077 | 39.0 | 32.95 | 0.58 |
| J103818-285307 | 31626 | 159.5743 | -28.8845 | 11.51 | 75 | 298 | 0.015784 | 73.1 | 34.32 | 0.58 |
| J103828-283056 | 740766 | 159.6196 | -28.5157 | 14.02 | 53 | 170 | 0.01568 | 80.1 | 34.52 | 0.58 |
| J103840-283405 | 31642 | 159.6679 | -28.5684 | 10.5 | 64 | 324 | 0.012725 | 53.8 | 33.65 | 0.58 |

| | | | | | | | | | | |
|----------------|---------|----------|----------|-------|----|-----|----------|-------|-------|------|
| J103858-300500 | 3758554 | 159.7422 | -30.084 | 15.49 | 64 | 81 | 0.013708 | 39.1 | 32.96 | 0.6 |
| J103902-291255 | 31664 | 159.7607 | -29.2144 | 14.11 | 63 | 165 | 0.011815 | 79.5 | 34.5 | 0.58 |
| J103905-265519 | 93061 | 159.7724 | -26.9228 | 12.91 | 66 | 351 | 0.036328 | 190.6 | 36.4 | 0.58 |
| J103918-265030 | 31683 | 159.8261 | -26.8421 | 10.34 | 72 | 345 | 0.011429 | 56.2 | 33.75 | 0.58 |
| J103922-293505 | 31690 | 159.8422 | -29.5846 | 11.69 | 49 | 275 | 0.014089 | 68.3 | 34.17 | 0.58 |
| J104000-292445 | 31732 | 160.0014 | -29.4123 | 13.2 | 66 | 184 | 0.013711 | 64.4 | 34.04 | 0.58 |
| J104004-301606 | 31738 | 160.0178 | -30.2679 | 10.6 | 66 | 287 | 0.012485 | 44.8 | 33.26 | 0.58 |
| J104058-274546 | 750199 | 160.2427 | -27.7623 | 14.52 | 67 | 163 | 0.014466 | 93.3 | 34.85 | 0.58 |
| J104059-270456 | 31805 | 160.2475 | -27.0819 | 9.65 | 56 | 397 | 0.016989 | 53.6 | 33.65 | 0.58 |
| J104100-284430 | 31809 | 160.2552 | -28.7418 | 12.3 | 56 | 193 | 0.013657 | 46.3 | 33.33 | 0.58 |
| J104139-254049 | | 160.4145 | -25.6805 | 14.66 | 55 | 123 | 0.014044 | 58.2 | 33.82 | 0.58 |
| J104139-274639 | 31852 | 160.4136 | -27.7778 | 13.86 | 60 | 136 | 0.015698 | 49.2 | 33.46 | 0.58 |
| J104157-264302 | | 160.4888 | -26.7174 | 13.7 | 63 | 256 | 0.037864 | 150.9 | 35.89 | 0.58 |
| J104239-300357 | | 160.6646 | -30.0664 | 16.12 | 70 | 82 | 0.009406 | 53.3 | 33.63 | 0.6 |
| J104245-264738 | 31924 | 160.6913 | -26.7937 | 12.55 | 58 | 345 | 0.036738 | 156.7 | 35.98 | 0.58 |
| J104252-252014 | | 160.7192 | -25.3373 | 13.87 | 49 | 126 | 0.022459 | 42.6 | 33.15 | 0.58 |
| J104311-261500 | 31951 | 160.7974 | -26.2501 | 10.2 | 61 | 431 | 0.016292 | 80.4 | 34.53 | 0.58 |
| J104326-251857 | 31960 | 160.859 | -25.316 | 13.62 | 49 | 125 | 0.01373 | 37.5 | 32.87 | 0.58 |
| J104339-285157 | 31981 | 160.913 | -28.8661 | 10.98 | 77 | 284 | 0.012715 | 52.2 | 33.59 | 0.58 |
| J104414-271548 | 757564 | 161.0589 | -27.2637 | 14.31 | 59 | 226 | 0.037798 | 157.4 | 35.99 | 0.58 |
| J104442-290119 | 734399 | 161.1761 | -29.0214 | 15.42 | 59 | 137 | 0.034775 | 102.4 | 35.05 | 0.58 |
| J104524-251723 | 780619 | 161.3536 | -25.2898 | 14.04 | 51 | 272 | 0.049468 | 196.9 | 36.47 | 0.58 |
| J104620-293733 | 727073 | 161.586 | -29.626 | 13.15 | 57 | 270 | 0.040611 | 128.8 | 35.55 | 0.58 |
| J104629-253308 | 32175 | 161.6229 | -25.5523 | 15.05 | 66 | 146 | 0.013183 | 96.6 | 34.92 | 0.59 |

Table A2: Norma HI data from WALLABY phase 1 pilot survey.

| Name | PGC | RA | DEC | W_{1tot} | i | W_{mx} | z_{cmb} | d_L | μ | e_μ |
|----------------|---------|----------|----------|------------|-----|----------|-----------|-------|-------|---------|
| J163435-620248 | 58527 | 248.6474 | -62.0468 | 12.65 | 63 | 235 | 0.015111 | 78.9 | 34.48 | 0.58 |
| J163749-621352 | 4077297 | 249.4542 | -62.2312 | 10.71 | 55 | 175 | 0.016254 | 18.5 | 31.34 | 0.58 |
| J163927-594844 | 3078607 | 249.8665 | -59.8123 | 12.06 | 67 | 472 | 0.037859 | 225.0 | 36.76 | 0.58 |
| J164107-605902 | 58755 | 250.2815 | -60.984 | 13.56 | 81 | 160 | 0.011866 | 58.2 | 33.82 | 0.59 |
| J164113-603202 | | 250.3072 | -60.5341 | 14.09 | 57 | 186 | 0.039869 | 98.3 | 34.96 | 0.58 |
| J164206-613441 | 3078658 | 250.5284 | -61.5783 | 14.28 | 71 | 192 | 0.017705 | 113.9 | 35.28 | 0.58 |
| J164249-610527 | 92488 | 250.7077 | -61.091 | 10.71 | 80 | 311 | 0.015065 | 55.0 | 33.7 | 0.58 |
| J164355-620233 | 349886 | 250.9815 | -62.0426 | 12.62 | 53 | 380 | 0.039332 | 193.3 | 36.43 | 0.58 |
| J164437-605103 | 58893 | 251.1563 | -60.8511 | 10.56 | 72 | 425 | 0.017819 | 92.3 | 34.83 | 0.58 |
| J164455-575030 | 3078727 | 251.2309 | -57.8417 | 12.33 | 47 | 401 | 0.048268 | 187.0 | 36.36 | 0.58 |
| J164508-611614 | | 251.2853 | -61.2707 | 13.14 | 79 | 172 | 0.012466 | 54.9 | 33.7 | 0.58 |
| J164727-575143 | 3078771 | 251.864 | -57.8622 | 13.25 | 63 | 362 | 0.04771 | 235.8 | 36.86 | 0.58 |
| J164739-570817 | 393557 | 251.9144 | -57.1381 | 14.49 | 55 | 83 | 0.002877 | 25.9 | 32.06 | 0.59 |
| J164749-613936 | | 251.9543 | -61.6602 | 12.85 | 64 | 174 | 0.017704 | 49.2 | 33.46 | 0.58 |
| J164826-623040 | 343635 | 252.1087 | -62.5112 | 11.99 | 63 | 185 | 0.014962 | 37.2 | 32.85 | 0.58 |
| J164911-620001 | 350325 | 252.2981 | -62.0004 | 12.63 | 58 | 276 | 0.05178 | 106.0 | 35.13 | 0.58 |
| J165131-603514 | 59130 | 252.8827 | -60.5873 | 12.64 | 65 | 134 | 0.011329 | 27.0 | 32.16 | 0.58 |
| J165439-605730 | | 253.6633 | -60.9586 | 14.13 | 69 | 169 | 0.010543 | 83.5 | 34.61 | 0.58 |
| J165455-610856 | 357773 | 253.7303 | -61.149 | 15.95 | 55 | 105 | 0.01483 | 79.0 | 34.49 | 0.59 |
| J165520-592615 | 3078940 | 253.8349 | -59.4375 | 13.57 | 75 | 153 | 0.016553 | 53.6 | 33.64 | 0.58 |
| J165559-592439 | 165948 | 253.9973 | -59.4109 | 11.8 | 48 | 265 | 0.016155 | 67.3 | 34.14 | 0.58 |
| J165632-594959 | 4584387 | 254.1346 | -59.8332 | 11.85 | 55 | 469 | 0.048021 | 202.3 | 36.53 | 0.58 |
| J165644-622413 | 4075676 | 254.1843 | -62.4038 | 9.94 | 64 | 377 | 0.017194 | 55.6 | 33.73 | 0.58 |
| J165645-620555 | | 254.1914 | -62.0988 | 15.66 | 58 | 196 | 0.030118 | 223.5 | 36.75 | 0.59 |
| J165840-582909 | 141869 | 254.6691 | -58.4859 | 11.08 | 55 | 307 | 0.020637 | 63.6 | 34.02 | 0.58 |
| J165847-612501 | | 254.6982 | -61.4117 | 14.35 | 74 | 161 | 0.015977 | 84.3 | 34.63 | 0.59 |
| J165934-623256 | 4080474 | 254.8947 | -62.549 | 10.55 | 57 | 256 | 0.016426 | 35.4 | 32.74 | 0.58 |
| J170039-584218 | 377019 | 255.1663 | -58.7052 | 13.55 | 69 | 184 | 0.020942 | 75.0 | 34.38 | 0.59 |
| J170116-621215 | 165971 | 255.3171 | -62.2043 | 12.1 | 55 | 406 | 0.046374 | 172.8 | 36.19 | 0.58 |
| J170149-603901 | 165952 | 255.4555 | -60.6504 | 12.28 | 65 | 290 | 0.016496 | 99.6 | 34.99 | 0.58 |
| J170232-584322 | 165953 | 255.6345 | -58.7229 | 11.58 | 60 | 315 | 0.020643 | 84.1 | 34.62 | 0.58 |
| J170349-595038 | | 255.9547 | -59.8441 | 13.09 | 49 | 253 | 0.01983 | 111.2 | 35.23 | 1.1 |
| J170700-600654 | 165955 | 256.7518 | -60.115 | 12.32 | 62 | 227 | 0.01436 | 63.9 | 34.03 | 0.58 |

| | | | | | | | | | | |
|----------------|--------|----------|----------|-------|----|-----|----------|-------|-------|------|
| J170747-595059 | 59659 | 256.9479 | -59.8499 | 11.77 | 79 | 281 | 0.015796 | 73.9 | 34.34 | 0.58 |
| J171120-603454 | 362143 | 257.8339 | -60.5819 | 14.33 | 50 | 95 | 0.016701 | 31.0 | 32.46 | 0.58 |
| J171134-610802 | | 257.8934 | -61.1341 | 16.58 | 55 | 98 | 0.009025 | 92.1 | 34.82 | 0.6 |
| J171309-603124 | 362690 | 258.2878 | -60.5234 | 13.56 | 70 | 125 | 0.016216 | 36.4 | 32.81 | 0.58 |
| J171339-615822 | 92494 | 258.4159 | -61.973 | 15.72 | 64 | 152 | 0.015052 | 142.7 | 35.77 | 0.59 |
| J171538-602409 | | 258.9097 | -60.4026 | 13.05 | 80 | 244 | 0.019515 | 101.9 | 35.04 | 0.58 |
| J171558-590923 | | 258.9944 | -59.1566 | 13.13 | 72 | 189 | 0.011865 | 65.3 | 34.07 | 0.58 |
| J171850-601104 | 365445 | 259.7118 | -60.1846 | 13.85 | 47 | 254 | 0.015513 | 158.6 | 36.0 | 0.58 |
| J171924-615016 | 92496 | 259.8532 | -61.838 | 13.3 | 75 | 276 | 0.024558 | 144.6 | 35.8 | 0.58 |

Table A3: Eridanus HI data from WALLABY phase 1 pilot survey.

| Name | PGC | RA | DEC | W_{1tot} | i | W_{mx} | z_{cmb} | d_L | μ | e_μ |
|----------------|--------|---------|----------|------------|-----|----------|-----------|-------|-------|---------|
| J034114-235017 | 13561 | 55.3083 | -23.8381 | 10.17 | 51 | 255 | 0.005911 | 29.3 | 32.33 | 0.58 |
| J033859-223502 | 13442 | 54.7458 | -22.5839 | 13.44 | 63 | 171 | 0.014086 | 62.5 | 33.98 | 0.58 |
| J034056-223350 | 13544 | 55.2333 | -22.5639 | 8.01 | 65 | 375 | 0.004788 | 22.6 | 31.77 | 0.58 |
| J034517-230001 | 13760 | 56.3208 | -23.0003 | 9.31 | 56 | 361 | 0.004831 | 38.3 | 32.92 | 0.58 |
| J034219-224520 | 13608 | 55.5792 | -22.7556 | 11.97 | 52 | 145 | 0.004856 | 23.3 | 31.83 | 0.58 |
| J033941-235054 | 13477 | 54.9208 | -23.8483 | 13.97 | 82 | 72 | 0.00503 | 15.3 | 30.92 | 0.58 |
| J034057-214245 | 13543 | 55.2375 | -21.7125 | 11.59 | 75 | 148 | 0.005277 | 20.2 | 31.52 | 0.58 |
| J034040-221711 | 13531 | 55.1667 | -22.2864 | 12.47 | 78 | 155 | 0.005533 | 32.8 | 32.58 | 0.58 |
| J034002-192200 | 13491 | 55.0083 | -19.3667 | 12.12 | 81 | 115 | 0.003657 | 15.9 | 31.01 | 0.58 |
| J034814-212824 | 13871 | 57.0583 | -21.4733 | 9.67 | 55 | 274 | 0.004936 | 26.8 | 32.14 | 0.58 |
| J034337-211418 | 13689 | 55.9042 | -21.2383 | 12.46 | 73 | 129 | 0.004994 | 23.3 | 31.83 | 0.58 |
| J034434-211123 | 135119 | 56.1417 | -21.1897 | 13.26 | 70 | 72 | 0.004884 | 11.2 | 30.25 | 0.58 |
| J034131-214051 | 13569 | 55.3792 | -21.6808 | 10.33 | 75 | 157 | 0.00507 | 12.7 | 30.52 | 0.58 |
| J033921-212450 | 13460 | 54.8375 | -21.4139 | 12.0 | 66 | 118 | 0.005032 | 15.9 | 31.0 | 0.58 |
| J033537-211742 | 13283 | 53.9042 | -21.295 | 11.8 | 79 | 144 | 0.005621 | 21.2 | 31.63 | 0.58 |
| J033341-212844 | 13184 | 53.4208 | -21.4789 | 8.99 | 49 | 265 | 0.005789 | 18.4 | 31.33 | 0.58 |
| J033347-192946 | 13190 | 53.4458 | -19.4961 | 10.2 | 55 | 231 | 0.006152 | 24.9 | 31.98 | 0.58 |
| J033810-194412 | 13401 | 54.5417 | -19.7367 | 12.69 | 72 | 176 | 0.013526 | 46.5 | 33.34 | 0.58 |
| J033757-213938 | 13392 | 54.4875 | -21.6606 | 13.66 | 74 | 137 | 0.013476 | 44.9 | 33.26 | 0.58 |
| J033147-211309 | 831121 | 52.9458 | -21.2192 | 14.49 | 65 | 102 | 0.013718 | 37.5 | 32.87 | 0.58 |
| J032455-214701 | 12762 | 51.2292 | -21.7836 | 12.9 | 55 | 102 | 0.004395 | 18.3 | 31.31 | 0.58 |
| J032425-213233 | 12737 | 51.1042 | -21.5425 | 8.5 | 73 | 342 | 0.004841 | 23.7 | 31.88 | 0.58 |
| J033527-211302 | 831168 | 53.8625 | -21.2172 | 12.92 | 48 | 120 | 0.004662 | 25.1 | 32.0 | 0.58 |
| J032735-211339 | 12889 | 51.8958 | -21.2275 | 11.37 | 77 | 165 | 0.005177 | 22.6 | 31.77 | 0.58 |
| J032831-222957 | 813307 | 52.1292 | -22.4992 | 13.71 | 74 | 70 | 0.005489 | 12.9 | 30.56 | 0.58 |
| J033653-245445 | 13342 | 54.2208 | -24.9125 | 12.27 | 59 | 124 | 0.005751 | 19.7 | 31.47 | 0.58 |
| J033302-240756 | 13154 | 53.2583 | -24.1322 | 12.71 | 76 | 159 | 0.005982 | 38.7 | 32.94 | 0.58 |
| J033728-243010 | 13368 | 54.3667 | -24.5028 | 7.97 | 51 | 231 | 0.004617 | 8.8 | 29.73 | 0.58 |
| J033617-253615 | 13304 | 54.0708 | -25.6042 | 11.54 | 67 | 125 | 0.004932 | 14.2 | 30.76 | 0.58 |
| J032937-232103 | 12986 | 52.4042 | -23.3508 | 13.1 | 76 | 115 | 0.005095 | 25.2 | 32.01 | 0.58 |
| J033326-234246 | 13171 | 53.3583 | -23.7128 | 9.57 | 76 | 257 | 0.005648 | 22.6 | 31.77 | 0.58 |
| J033228-232245 | 13127 | 53.1167 | -23.3792 | 13.5 | 56 | 70 | 0.005438 | 11.7 | 30.34 | 0.58 |

Table A4: NGC4636 HI data from WALLABY phase 1 pilot survey.

| Name | PGC | RA | DEC | W_{1tot} | i | W_{mx} | z_{cmb} | d_L | μ | e_μ |
|----------------|---------|----------|---------|------------|-----|----------|-----------|-------|-------|---------|
| J122708+055255 | 40801 | 186.7869 | 5.8821 | 10.78 | 80 | 166 | 0.004854 | 17.4 | 31.2 | 0.58 |
| J122713-020236 | 40820 | 186.8062 | -2.0436 | 12.02 | 65 | 83 | 0.022686 | 8.2 | 29.57 | 0.58 |
| J122729+073841 | 40861 | 186.8728 | 7.6449 | 12.14 | 58 | 141 | 0.00402 | 23.8 | 31.88 | 0.58 |
| J122745+013601 | 135803 | 186.9391 | 1.6004 | 15.47 | 48 | 67 | 0.005481 | 26.7 | 32.13 | 0.6 |
| J122755+054312 | 40933 | 186.9813 | 5.7202 | 11.34 | 77 | 138 | 0.008644 | 15.8 | 31.0 | 0.58 |
| J122852+041739 | 41088 | 187.2186 | 4.2942 | 11.43 | 81 | 289 | 0.015287 | 66.8 | 34.12 | 0.58 |
| J122930+074142 | 41170 | 187.3766 | 7.6952 | 11.0 | 67 | 191 | 0.003635 | 24.9 | 31.98 | 0.58 |
| J122932+005020 | 41177 | 187.385 | 0.8391 | 14.34 | 75 | 121 | 0.008622 | 49.3 | 33.46 | 0.58 |
| J123021-013813 | 3294304 | 187.5902 | -1.6372 | 15.84 | 60 | 73 | 0.00828 | 37.6 | 32.88 | 0.59 |
| J123022+034431 | 41307 | 187.592 | 3.7422 | 10.84 | 78 | 317 | 0.01526 | 60.6 | 33.91 | 0.58 |

| | | | | | | | | | | |
|----------------|---------|----------|---------|-------|----|-----|----------|-------|-------|------|
| J123026+041450 | 41317 | 187.6114 | 4.2472 | 9.59 | 54 | 386 | 0.015258 | 49.2 | 33.46 | 0.58 |
| J123132+071828 | 5060276 | 187.8843 | 7.3078 | 13.75 | 70 | 182 | 0.02555 | 80.6 | 34.53 | 0.58 |
| J123156+035316 | 97234 | 187.9865 | 3.8878 | 13.74 | 59 | 166 | 0.016135 | 67.8 | 34.16 | 0.58 |
| J123209-010543 | 1126897 | 188.0407 | -1.0955 | 14.41 | 68 | 130 | 0.009177 | 58.3 | 33.83 | 0.58 |
| J123228+002315 | 4105156 | 188.1171 | 0.3877 | 10.07 | 58 | 173 | 0.006247 | 13.4 | 30.64 | 0.58 |
| J123236+023943 | 41599 | 188.153 | 2.6622 | 11.49 | 81 | 139 | 0.006931 | 17.1 | 31.16 | 0.58 |
| J123244+000656 | 41618 | 188.1867 | 0.1157 | 7.08 | 83 | 303 | 0.004902 | 9.8 | 29.96 | 0.58 |
| J123249+031748 | 41625 | 188.2064 | 3.2967 | 12.05 | 52 | 241 | 0.017795 | 62.8 | 33.99 | 0.58 |
| J123250+054744 | 41627 | 188.21 | 5.7957 | 12.66 | 48 | 283 | 0.040532 | 112.8 | 35.26 | 0.58 |
| J123257+043441 | 41647 | 188.2394 | 4.5781 | 13.64 | 62 | 81 | 0.005243 | 16.5 | 31.08 | 0.58 |
| J123320+013119 | 41700 | 188.3373 | 1.522 | 12.89 | 67 | 73 | 0.00673 | 9.6 | 29.91 | 0.58 |
| J123329+034732 | 41716 | 188.3711 | 3.7923 | 12.6 | 56 | 104 | 0.004143 | 16.5 | 31.08 | 0.58 |
| J123407+023905 | 6656564 | 188.5313 | 2.6514 | 6.67 | 78 | 363 | 0.006928 | 11.5 | 30.29 | 0.58 |
| J123422+021914 | 41816 | 188.5928 | 2.3207 | 10.9 | 79 | 116 | 0.007036 | 9.3 | 29.85 | 0.58 |
| J123427+021108 | 41823 | 188.6148 | 2.1857 | 7.18 | 70 | 333 | 0.00716 | 12.3 | 30.44 | 0.58 |
| J123554-015112 | 41998 | 188.9783 | -1.8534 | 12.73 | 55 | 264 | 0.024126 | 102.4 | 35.05 | 0.58 |
| J123555-025405 | 41982 | 188.9812 | -2.9016 | 11.47 | 51 | 316 | 0.024926 | 80.2 | 34.52 | 0.58 |
| J123609+073152 | 1324268 | 189.039 | 7.5313 | 11.83 | 48 | 363 | 0.025156 | 123.8 | 35.46 | 0.58 |
| J123630+001315 | 1160233 | 189.1273 | 0.2208 | 13.88 | 53 | 171 | 0.013554 | 76.4 | 34.42 | 0.58 |
| J123641+030621 | 42080 | 189.1734 | 3.106 | 13.5 | 71 | 127 | 0.00594 | 36.5 | 32.81 | 0.58 |
| J123651-003515 | 1139671 | 189.2162 | -0.5877 | 15.17 | 50 | 70 | 0.009718 | 25.4 | 32.03 | 0.58 |
| J123703+065533 | 42108 | 189.2635 | 6.926 | 11.7 | 55 | 101 | 0.006584 | 10.4 | 30.08 | 0.58 |
| J123734+042150 | 42152 | 189.3924 | 4.3641 | 10.66 | 57 | 205 | 0.01881 | 24.3 | 31.93 | 0.58 |
| J123742-033505 | 42153 | 189.428 | -3.585 | 17.17 | 62 | 76 | 0.025254 | 74.2 | 34.35 | 0.6 |
| J123748-012038 | 42173 | 189.4502 | -1.3441 | 12.95 | 51 | 68 | 0.006298 | 8.7 | 29.69 | 0.58 |
| J123802+001036 | 1159012 | 189.5112 | 0.1767 | 15.02 | 47 | 140 | 0.014576 | 87.9 | 34.72 | 0.58 |
| J123805-000137 | 42202 | 189.5225 | -0.027 | 10.65 | 65 | 344 | 0.013658 | 64.7 | 34.05 | 0.58 |
| J123805-002419 | 1144183 | 189.524 | -0.4053 | 14.95 | 75 | 185 | 0.026609 | 144.7 | 35.8 | 0.61 |
| J123827+041912 | 42241 | 189.6154 | 4.32 | 8.41 | 71 | 255 | 0.003761 | 13.1 | 30.59 | 0.58 |
| J123835+012413 | 42255 | 189.6482 | 1.4036 | 11.75 | 76 | 292 | 0.018488 | 78.9 | 34.48 | 0.58 |
| J123912+060038 | 42319 | 189.802 | 6.0106 | 10.06 | 56 | 350 | 0.009212 | 50.9 | 33.54 | 0.58 |
| J123917-003149 | 42336 | 189.8223 | -0.5305 | 9.41 | 74 | 201 | 0.004704 | 13.2 | 30.6 | 0.58 |
| J123922+045608 | 42340 | 189.8425 | 4.9358 | 12.31 | 49 | 113 | 0.006518 | 17.0 | 31.15 | 0.58 |
| J123928+041549 | 42354 | 189.8694 | 4.2638 | 12.27 | 70 | 278 | 0.050267 | 91.1 | 34.8 | 0.58 |
| J123949+014016 | 42393 | 189.9577 | 1.6711 | 12.05 | 62 | 108 | 0.005214 | 13.6 | 30.67 | 0.58 |
| J124002-010258 | 1128047 | 190.0119 | -1.0494 | 13.44 | 65 | 77 | 0.006467 | 13.8 | 30.7 | 0.58 |
| J124002-033623 | 42409 | 190.009 | -3.6066 | 13.62 | 60 | 114 | 0.009627 | 31.6 | 32.5 | 0.58 |
| J124109+041725 | 1266160 | 190.288 | 4.2904 | 14.44 | 78 | 99 | 0.029993 | 35.1 | 32.73 | 0.59 |
| J124111-013526 | 42538 | 190.2959 | -1.5906 | 12.87 | 61 | 206 | 0.01448 | 68.2 | 34.17 | 0.58 |
| J124111+012435 | 42542 | 190.2983 | 1.4099 | 11.64 | 52 | 212 | 0.006805 | 40.8 | 33.05 | 0.58 |
| J124121+001315 | 1160198 | 190.3405 | 0.2211 | 15.64 | 65 | 142 | 0.017147 | 119.8 | 35.39 | 0.62 |
| J124123-030327 | 42559 | 190.3462 | -3.0577 | 11.55 | 66 | 99 | 0.005977 | 9.2 | 29.81 | 0.58 |
| J124128-031517 | 91219 | 190.3698 | -3.2547 | 14.84 | 73 | 111 | 0.007142 | 52.4 | 33.6 | 0.58 |
| J124232-000459 | 42689 | 190.6361 | -0.0832 | 8.79 | 64 | 239 | 0.006877 | 13.9 | 30.71 | 0.58 |
| J124237-020708 | 3106365 | 190.6565 | -2.1189 | 14.53 | 48 | 266 | 0.047148 | 236.8 | 36.87 | 0.58 |
| J124240+012047 | 42709 | 190.6693 | 1.3465 | 11.1 | 54 | 326 | 0.017886 | 71.9 | 34.28 | 0.58 |
| J124257-011345 | 42747 | 190.7395 | -1.2294 | 10.36 | 77 | 316 | 0.011848 | 48.2 | 33.41 | 0.58 |
| J124317-003841 | 42791 | 190.8234 | -0.6449 | 10.26 | 72 | 304 | 0.009962 | 42.6 | 33.15 | 0.58 |
| J124333+014827 | 92947 | 190.8877 | 1.8077 | 12.33 | 62 | 174 | 0.049606 | 38.5 | 32.93 | 0.58 |
| J124350-003344 | 42847 | 190.9608 | -0.5624 | 9.55 | 48 | 266 | 0.009907 | 23.9 | 31.89 | 0.58 |
| J124421+042536 | 42892 | 191.0894 | 4.4267 | 12.06 | 61 | 304 | 0.029722 | 97.9 | 34.95 | 0.58 |
| J124428-030017 | 42909 | 191.1179 | -3.0048 | 11.18 | 50 | 453 | 0.025035 | 139.1 | 35.72 | 0.58 |
| J124428+002815 | 42910 | 191.119 | 0.4709 | 10.97 | 79 | 104 | 0.005064 | 7.8 | 29.45 | 0.58 |
| J124433-021916 | 42921 | 191.141 | -2.3212 | 12.97 | 55 | 134 | 0.00644 | 31.6 | 32.5 | 0.58 |
| J124508-002747 | 42975 | 191.2845 | -0.4632 | 6.7 | 66 | 422 | 0.006194 | 15.4 | 30.94 | 0.58 |
| J124531-003203 | 3110155 | 191.3824 | -0.5343 | 10.52 | 59 | 157 | 0.006527 | 13.8 | 30.7 | 0.58 |
| J124548-002600 | 1143451 | 191.4504 | -0.4335 | 13.92 | 54 | 74 | 0.0067 | 16.1 | 31.03 | 0.58 |
| J124608+042643 | 1268285 | 191.5344 | 4.4453 | 14.12 | 66 | 229 | 0.024736 | 147.8 | 35.85 | 0.58 |
| J124651-013308 | 3295908 | 191.7129 | -1.5524 | 15.04 | 57 | 69 | 0.024029 | 23.5 | 31.86 | 0.59 |
| J124701-013444 | 43128 | 191.7543 | -1.5789 | 12.17 | 50 | 199 | 0.01022 | 46.2 | 33.33 | 0.58 |
| J124717+002405 | 43153 | 191.821 | 0.4016 | 11.09 | 61 | 156 | 0.047582 | 17.8 | 31.25 | 0.58 |
| J124753-011107 | 43198 | 191.9724 | -1.1853 | 11.89 | 70 | 349 | 0.02459 | 118.2 | 35.36 | 0.58 |

| | | | | | | | | | | |
|----------------|---------|----------|--------|-------|----|-----|----------|------|-------|------|
| J124800+042609 | 3994854 | 192.0002 | 4.4358 | 12.53 | 56 | 155 | 0.004509 | 34.1 | 32.67 | 0.58 |
| J125038+012749 | 43470 | 192.6614 | 1.4636 | 10.89 | 81 | 175 | 0.005355 | 20.2 | 31.53 | 0.58 |
| J124808+033759 | 5808028 | 192.0334 | 3.6333 | 14.96 | 55 | 93 | 0.024668 | 39.6 | 32.99 | 0.7 |

This paper has been typeset from a $\text{\TeX}/\text{\LaTeX}$ file prepared by the author.